


## Research Article

# Exploring morphological evolution in relation to habitat moisture in the moss genus *Fissidens* using molecular data generated from herbarium specimens

Jessica M. Budke<sup>1†\*</sup> , Nikisha R. Patel<sup>1,2,3†</sup>, GoFlag Consortium<sup>4†</sup>, Mark D. Wienhold<sup>1,5</sup>, and Maria A. Bruggeman-Nannenga<sup>6</sup>

<sup>1</sup>University of Tennessee, Knoxville, TN 37996, USA

<sup>2</sup>University of Connecticut, Storrs, CT 06269, USA

<sup>3</sup>Trinity College, Hartford, CT 06106, USA

<sup>4</sup>University of Florida, Gainesville, FL 32611, USA

<sup>5</sup>490 BioTech, Knoxville, TN 37996, USA

<sup>6</sup>Griffensteynseplein 23, 3703 NL BE Zeist, The Netherlands

<sup>†</sup>Co-first authors with equal contribution.

<sup>‡</sup>GoFlag is an NSF-funded project (DEB-1541506) based at the University of Florida, Field Museum, and University of Arizona. Project personnel include (at UF): J. Gordon Burleigh, Emily Sessa, Stuart McDaniel, Christine Davis, Pavlo Antonenko, Sarah Carey, Lorena Endara, Weston Testo; (at Field): Matt von Konrat, Eve Gaus; (at UA): Hong Cui.

\*Author for correspondence. E-mail: jbudke@utk.edu

Received 11 May 2022; Accepted 25 October 2022; Article first published online 31 October 2022

**Abstract** Morphological evolution in mosses has long been hypothesized to accompany shifts in microhabitats, which can be tested using comparative phylogenetics. These lines of inquiry have been developed to include target capture sequencing, which can yield phylogenomic scale data from herbarium specimens. Here, we test the relationship between taxonomically important morphological characters in the moss genus *Fissidens*, using a 400-locus data set generated using a target-capture approach in tandem with a three-locus phylogeny generated using Sanger sequencing. Phylogenetic trees generated using ASTRAL and Bayesian inference were used to test the monophyly of subgenera/sections. These trees provide the basis for ancestral character state reconstructions and phylogenetic correlation analyses for five morphological characters and characters related to the moisture habitat, scored from the literature and by specimen inspection. Many of these characters exhibit statistically significant phylogenetic signal. Significant correlations were found between the limbidium (phylloid/leaf border of the gametophyte) and habitat moisture niche breadth, which could be interpreted as the more extensive limbidium enabling species to survive across a wider variety of habitats. We also found correlations between costa anatomy, peristome morphology, and the limbidium, which could reflect the evolutionary recruitment of genetic networks from the gametophyte to the sporophyte phase. The correlation found between average habitat moisture and the sexual system indicates that dioicous and polyoicous species are more likely to be found in moist habitats and that these higher moisture levels could be particularly, reproductively advantageous to species with separate sexes.

**Key words:** ancestral character reconstruction, axillary hyaline nodules, classification system, costa anatomy, habitat moisture, limbidium, peristome teeth, sexual system.

## 1 Introduction

Morphology has long been foundational to our understanding of relationships between species (e.g., Endress et al., 2000; Pelter et al., 2004). The advent of molecular systematics opened up avenues to use DNA data to test morphological hypotheses regarding these relationships (e.g., Felsenstein, 2004; Cox, 2018). Next-generation sequencing technologies have enabled us to build phylogenetic

trees based on data from hundreds of genes using small amounts of tissue from natural history specimens (e.g., Liu et al., 2019; Folk et al., 2021). Employing a process of reciprocal illumination, we are able to then return to the morphology to evaluate its ability to uncover synapomorphies as key features for defining clades (e.g., Nicolalde-Morejón et al., 2009; Medina et al., 2013). Morphological reduction has been shown to be rampant across mosses, particularly for structures such as the peristome, seta, and

costa, and has been hypothesized to accompany shifts in microhabitat (e.g., movement from terrestrial to aquatic or terrestrial to epiphytic habitats; see Schofield, 1981; Vitt, 1981; Buck, 1994), but correlations between habitat and morphological characters across moss species in many studies are not highly supported (Hedenäs, 2001; Olsson et al., 2009; Huttunen et al., 2012). Transitions in gametophyte sexual systems have also been used as a defining feature for clades of mosses (e.g., McDaniel & Perroud, 2012). Examining the relationship between morphology and microhabitat features in a phylogenetic context can enable us to identify homoplasious and homologous morphologies and evaluate correlations between these features in light of evolution (e.g., Huttunen et al., 2018).

Fissidentaceae Schimp. is a broadly distributed moss family composed of approximately 440 named species that are all currently in the genus *Fissidens* Hedw. (Crosby et al., 2000). Species diversity is higher in tropical regions; as an example, only 37 *Fissidens* species are described for temperate North America (Flora of North America, 2007), whereas 93 *Fissidens* species are described for tropical areas of the Americas, including 58 endemic species (Pursell, 2007). The genus encompasses terrestrial, semiaquatic, and fully aquatic species and examples of each are known from both temperate and tropical regions (Sharp & Crum, 1994; Seppelt & Stone, 2016). However, little is known about the evolutionary transitions between terrestrial and aquatic habitats in *Fissidens*, including the number of times these transitions have occurred, or the relationship between these transitions in habitat to both morphological and reproductive characters.

*Fissidens* is distinguished morphologically from other mosses by gametophytes that have a lenticular apical cell at maturity (Chamberlin, 1980), which produces an equitant phyllid arrangement. Each phyllid (leaf-like structure) consists of a vaginant lamina that clasps the caulid (stem-like structure), forming a pocket, along with a dorsal and apical lamina. The vaginant lamina is interpreted as homologous to the “true leaf” of other related mosses, whereas the dorsal and apical lamina are understood to be outgrowths (Mishler, 1988). This phyllid morphology is nearly uniform across the genus, whereas the presence or absence of the axillary hyaline nodules, costa (midrib), and limbidium (border) is more variable. The sexual system, as defined in Crawford et al. (2009), also varies across *Fissidens* species, which range from monoicous (including autoicous, cladautoicous, gonioautoicous, and rhizautoicous) to dioicous (including phyllodioicous, pseudautoicous, and pseudomonocous) to polyoicous (Smith & Smith, 2004; Flora of North America, 2007; Pursell, 2007). *Fissidens* sporophytes have a haplolepidous peristome, consisting of a single ring of 16 endostome teeth, with the upper part of the teeth typically divided into two filaments (Edwards, 1979). Phylogenetic studies of this group indicate a close affinity with Dicranaceae Schimp. (Goffinet & Cox, 2000; LaFarge et al., 2000); however, the precise relationships between Fissidentaceae and other families in Dicranidae Doweld remain ambiguous (Stech et al., 2012; Cox et al., 2014; Fedosov et al., 2016; Liu et al., 2019; Bonfim Santos et al., 2021).

Infrageneric classification systems for *Fissidens* have a long history of scientific discourse and discussion. The original systems were proposed by Müller (1848, 1851, 1900) and Brothierus (1901, 1924); Müller based his system on gametophyte morphology, whereas Brothierus added a focus on sporophyte peristome morphology. These systems were revised in a series of studies by Potier de la Varde (1931), Norkett (1969), Bruggeman-Nannenga (1974, 1978), Iwatsuki (1985), Pursell (1987), Pursell et al. (1988), Bruggeman-Nannenga & Berendsen (1990), Pursell & Bruggeman-Nannenga (2004), and Suzuki & Iwatsuki (2007), with the majority of these studies focusing on key morphological characters associated with the axillary hyaline nodules, costa anatomy, limbidium, and peristome teeth (for a summary of these systems, see table 1 in Suzuki & Iwatsuki, 2007). The resulting classification systems range in complexity from Pursell (1987), who defined four *Fissidens* subgenera and seven sections, to Bruggeman-Nannenga & Berendsen (1990) who recognized the second genus in Fissidentaceae, *Nanobryum* Dixon, as well as five subgenera and ten sections in the genus *Fissidens*. In addition to the morphological characters listed above, Iwatsuki (1985) and Suzuki & Iwatsuki (2007) integrated chromosome numbers into their analyses and proposed a relationship between the ploidy level and sexual system in *Fissidens*, whereas Pursell & Bruggeman-Nannenga (2004) included the number of files of exothecial cells in the capsule wall and the papilosity of the lamina cells in their system. The most recent revision of the infrageneric classification system for *Fissidens* was the first based on the analysis of DNA sequence data (Suzuki et al., 2018). They refined the system of Suzuki & Iwatsuki (2007) by analyzing the evolution of axillary hyaline nodules, chromosome number, costa anatomy, limbidium, peristome teeth, and sexual system across *Fissidens* phylogeny, and also used these features to define three subgenera and seven sections in the genus. While their study was groundbreaking in the establishment of the first molecular phylogeny for *Fissidens* and their analysis of morphological characters using the phylogeny, it was limited by its use of only two plastid loci (*rbcL*, *rps4*) to construct the phylogenetic tree and their restricted geographic sampling that included three specimens from Laos, two from French Polynesia, one from the United Kingdom, and all others from Japan.

In this study, we constructed two complementary data sets using herbarium specimens collected from around the world to examine relationships in the genus *Fissidens*. Next-generation sequencing technologies were used to assemble a data set of over 400 loci for approximately 40 *Fissidens* species. In parallel, we assembled a three-loci data set (*trnL-F*, *trnA-nad7*, *ITS2*) for over 100 samples representing approximately 50 *Fissidens* species using Sanger sequencing methods. These phylogenetic trees are used to address the following questions: (i) Focusing on the classification systems of Pursell & Bruggeman-Nannenga (2004) and Suzuki et al. (2018), do the subgenera and sections proposed for *Fissidens* correspond to monophyletic lineages? (ii) Using phylogenetic comparative methods, do the key morphological characters used to define *Fissidens* infrageneric classification systems, including axillary hyaline nodules, costa anatomy, limbidium, peristome teeth, and sexual system have significant phylogenetic signals and are these characters correlated

with each other? (iii) Are *Fissidens* morphological features correlated with the habitat moisture level across the phylogeny? By addressing these questions, we aim to expand our understanding of morphological evolution in Fissidentaceae.

## 2 Material and Methods

### 2.1 Taxon sampling

We selected specimens with the aim of representing species diversity across the genus *Fissidens* and within each subgenus and section based on the classification system of Pursell & Bruggeman-Nannenga (2004). Further, when choosing species, we paid attention to unusual habitat preferences (such as those that are fully aquatic, or with strictly northern temperate distributions). Ultimately, each subgenus and section in the Pursell & Bruggeman-Nannenga (2004) classification scheme was sampled and is represented in the phylogenies, with the exception of subgenus *Fissidens* section *Sarawakia* (Müll. Hal.) Pursell & Brugg.-Nann. (Table S1). We categorized species according to the morphology-based classification system of Pursell & Bruggeman-Nannenga (2004) and the classification system of Suzuki et al. (2018) and compared and contrasted these two systems (Table S2).

### 2.2 Character scoring

We scored habitat moisture level, sexual system, and four morphological characters for the Fissidentaceae species to reconstruct ancestral states, assess phylogenetic signals and test for correlations between characters. For nonmorphological characters, the states were determined from descriptions in the literature (Table S1). Morphological character states were determined either from the literature or by examining the herbarium specimens used in the study (Table S1). Habitat moisture was scored using the Ellenberg values for moisture (table 13 in Hill et al., 2007), a scale that divides habitat moisture into 12 levels (ordered categorical variable) from “extreme dryness, restricted to situations that often dry out for some time” (level 1) to “moist soils or rock or bark in humid places” (level 6) to “normally submerged” (level 12). Minimum and maximum moisture levels were determined by applying the Ellenberg values to published moisture descriptions from the literature for each species. The average moisture level was calculated using these minimum and maximum values. Habitat moisture niche breadth (continuous variable) was also calculated as the difference between the habitat moisture minimum and habitat moisture maximum moisture levels for a species. The sexual system was scored as monoicous, dioicous, or polyicous (categorical variable with three states). Species scored as polyicous are those for which literature sources conflict, suggesting that monoicy and dioicy are both possible. Uncertain descriptions that could not be placed into one of these categories, and species where the sexual system is not reported in the literature, were scored as unknown and left as missing data.

Axillary hyaline nodules, which are clusters of inflated branch primordia cells, were scored as absent, weakly developed, or well-developed (categorical variable). Limbidia are borders of elongated cells located on the phyllid margin.

For this character, species were scored as having one of five states on the nonperichaetial, vegetative leaves; (i) elimbate, (ii) elimbate to partially limbate on vaginant lamina, (iii) limbate on proximal half of vaginant lamina to fully limbate on vaginant lamina, (iv) fully limbate on vaginant lamina and limbidium extending beyond onto the apical lamina, or (v) limbate on all regions of the lamina (categorical variable). Costa anatomy was scored using the system of Pursell & Bruggeman-Nannenga (2004) as having one of three types: *bryoides*, *taxifolius*, or *oblongifolius* (categorical variable). Peristome morphology was scored using two different systems that define the teeth using morphological criteria; the first system includes eight of the peristome types (*anomalous*, *bryoides*, *fasciculatus*, *nobilis*, *scariosus*, *similir-etis*, *taxifolius*, *zippelianus*; categorical variable) outlined in Bruggeman-Nannenga & Berendsen (1990) and the second system includes five peristome types (*Fissidens*, *Moenkemeyera*, *Neoambylohallia*, *Octodicerias*, *Pachyfissidens*; categorical variable) as outlined in Suzuki and Iwatsuki (2007).

### 2.3 GoFlag data set—DNA extraction, sequence capture, and sequencing

Between seven and 20 mg of tissue were sampled from each herbarium specimen, which had collection dates ranging from 1991 to 2015 (Table S1). These samples were submitted to the GoFlag project at the University of Florida for DNA extraction, library construction, targeted enrichment, and sequencing as detailed in Breinholt et al. (2021).

### 2.4 Bioinformatic processing and phylogenetic analyses of GoFlag data set

Targeted loci were recovered from target-enriched libraries sequenced on the Illumina HiSeq. 3000 platform, using the six-step pipeline of Breinholt et al. (2021; modified from Breinholt et al., 2018), which includes (i) trimming reads, (ii) assembly, (iii) probe trimming, (iv) inferring orthology to reference, (v) contamination filtering, and (vi) alignment and merging isoforms. We then removed all reads associated with a given locus if there were multiple variants, to minimize issues of paralogy. The GoFlag 451 and 408 probe sets and scripts used for the bioinformatic processing are available on Dryad (Breinholt et al., 2020).

We conducted phylogenetic analyses using two sets of data: (i) the probe data set that includes only conserved exon regions targeted by the sequencing probes, an average of 200 bp in length; (ii) the full data set that included both conserved exon regions from the probe data set and flanking intron regions, on average 1200 bp in length. For both data sets, we conducted analyses of a concatenated supermatrix of all the loci and also of individual loci to build gene trees that were then used to construct species trees using a multispecies coalescent approach (MSC); see below (data available on Dryad, doi:10.5061/dryad.gtht76hpg; Figs. S1–S6).

For a given locus, if we recovered sequences for less than 20% of the samples (i.e., fewer than 10), we removed that locus from further analysis. The alignments were then pruned to include only sites (i.e., columns in each aligned matrix) that had data from 10 or more samples. Partition-Finder2 (Lanfear et al., 2016) was used to analyze each locus to determine the optimal number of partitions for the concatenated analyses. We ran a maximum likelihood (ML)

search with 1000 rapid bootstrap replicates with the GTRGAMMA substitution model for all partitions using RAxML 8.2.12 (Stamatakis, 2014). The concatenated analyses were implemented using the CIPRES Science Gateway (Miller et al., 2010). Each locus was also analyzed independently using ML with 200 rapid bootstrap replicates under the GTRGAMMA substitution model using RAxML. The scripts used to process the data for phylogenetic analyses and supermatrix alignments with locus boundaries are available on Dryad (doi:10.5061/dryad.gtht76hpg).

Prior to species-tree inference based on the MSC approach, we used the `sumtrees.py` script in DendroPy (Sukumaran & Holder, 2010) to remove any branches in each of the gene trees that had less than 33% bootstrap support, to reduce the effect of uncertainty within individual gene trees. We used default parameters in ASTRAL v5.7.3 (Sayyari & Mirarab, 2016) to estimate the species tree from these gene trees. Branch support was evaluated using both the local posterior probability (LPP) method, which estimates the relative quartet support on each branch, and the multi-locus bootstrap (MLBS) method (Seo, 2008), which samples the gene tree phylogenies using 100 replicates.

Gene tree congruence and conflict were also evaluated using a bipartition analysis in PhyParts (Smith et al., 2015). The ASTRAL species tree was rooted using *Ceratodon purpureus* (Hedw.) Brid. PhyParts was then used to calculate the number of gene trees supporting each bipartition in the species tree, plotted in pie charts on each node. The summary and visualization were carried out using the ETE Python package (Huerta-Cepas et al., 2016) with scripts available from [github.com/mossmatters/phyloscripts](https://github.com/mossmatters/phyloscripts) (Medina et al., 2019).

## 2.5 Three-gene data set—DNA extraction, amplification, and sequencing

We performed DNA extraction, amplification, and sequencing for the three genes used in the concatenated phylogenetic analysis. Between 0.4 and 18 mg of tissue were sampled from each specimen. DNA was extracted using the DNeasy Plant Mini Kit (Qiagen, Venlo, the Netherlands). Three DNA regions were amplified using polymerase chain reaction (PCR): (i) the coding region of the mitochondrial gene *trnA*; (ii) the noncoding region between the chloroplast genes *trnL* and *trnF* (*trnL-F*), and; (iii) *ITS2*, the nuclear ribosomal spacer region between 5.8S and 26S rDNA genes. We used primers designed in previous studies (*trnA*, Wahrmond et al., 2008; *trnL-F*, Frey et al., 1999; *ITS2*, Stech & Frahm, 1999). The same primers were used for both PCR amplification and sequencing. Amplification was implemented in Eppendorf Mastercycler thermal cyclers (Eppendorf, Hamburg, Germany) in 25  $\mu$ L reactions, which included the following: 12.5  $\mu$ L of Acustart II Supermix (Quantabio, Beverly, MA, USA), 9.3  $\mu$ L of water, 0.6  $\mu$ L of each primer, and 2  $\mu$ L of sample DNA. Amplified DNA was visualized on a 1% agarose gel stained with ethidium bromide and a 1 kb plus ladder (Thermo Fisher Scientific, Waltham, MA, USA), excised from gels, and purified using QIAEX II Gel Extraction Kit (Qiagen). The DNA concentration was evaluated using a DynaQuant Fluorometer (Hoefer, Holliston, MA, USA) and samples with greater than 1 ng/ $\mu$ L were sequenced. Amplification products were sequenced using BigDye version

3.1 (Applied Biosystems, Foster City, CA, USA) on a 3730 Genetic Analyzer (Applied Biosystems).

## 2.6 Analysis of the three-gene data set

We used Geneious 10.1.3 (<https://www.geneious.com>) to trim reads (.ab1 files) at the 5'- and 3'-ends of each sequence to remove ambiguous base calls. Forward and reverse orientation reads were assembled using *de novo* assembly, and then used to generate consensus sequences for each species. Consensus sequences were aligned using ClustalW 2.1 (Larkin et al., 2007) using an IUB cost matrix with 10 gaps open and 5 gap extension penalties. Individual gene alignments were concatenated to produce a single matrix. The data were partitioned by region and optimal evolutionary models were selected for each using jModelTest 2 (Darriba et al., 2012; Table S3). Bayesian inference (BI) for phylogenetic analysis was implemented in MrBayes 3.2.7 (Huelsenbeck & Ronquist 2001) using CIPRES (Miller et al., 2010). MrBayes was run for five million generations with four heated chains. The first 500 000 trees were discarded as burn-in. The remaining trees were used to construct a majority-rule consensus tree with posterior probability (PP) support values.

## 2.7 Ancestral state reconstructions

The ancestral states for four morphological characters, habitat moisture level, and sexual system were inferred using ML for the three-gene Bayesian phylogeny. The characters axillary hyaline nodules, limbidium, costa anatomy, peristome morphology (scored using both the Bruggeman-Nannenga & Berendsen (1990) and Suzuki & Iwatsuki (2007) systems), and sexual system were analyzed as discrete characters, whereas habitat moisture (minimum, average maximum, and specialization) was analyzed as a continuous character. For the discrete characters, three models of character evolution (“ER”—equal rates, “SYM”—symmetric, “ARD”—all rates different) were tested for fit on the basis of negative log-likelihood using the “fitDiscrete” function in GEIGER (Harmon et al., 2008; Table S4) implemented in R version 4.0.2 (R Core Team, 2020) and RStudio 1.0.143 (RStudio Team, 2020). For the characters axillary hyaline nodules and limbidium, the fit of an ordered model, comprising a transition rate matrix restricting evolutionary transitions between adjacent character states (e.g.,  $1 < \rightarrow 2 < \rightarrow 3$ ) was tested in comparison to multiple unordered models (Table S4). There was no significant difference among tested models and so the simplest model (equal rates) was used in each case for subsequent likelihood-based character mapping and ancestral character state reconstruction in *phytools* using the function “ace” (Cunningham et al., 1998).

The function “lik.anc” implemented in *phytools* was used to determine the marginal ancestral states for the discrete characters. For the four continuous moisture-related characters (maximum habitat moisture, minimum habitat moisture, average habitat moisture, and habitat moisture niche breadth), the function “fitContinuous” was used to model and reconstruct ancestral states. The three-gene tree was rooted using *C. purpureus* and converted to an ultrametric tree for the reconstructions. None of the four non-*Fissidens* taxa were included in the ancestral character state

reconstructions. The resulting reconstructions were visualized using the packages *ggtree* (Yu, 2020) and *ape* (Paradis & Schliep, 2019). The likelihood values given for states at each node were used to infer the most likely ancestral states. A likelihood value for a given state that is greater than 0.90 is considered very high, greater than 0.75 is considered high, and greater than 0.5 is considered low.

### 2.8 Phylogenetic signal and correlation analysis

The phylogenetic signal was calculated using the three-gene Bayesian phylogeny for each character analyzed for the ancestral character-state reconstructions. The functions “fitDiscrete” and “fitContinuous” from the package GEIGER (Harmon et al., 2008) were implemented in R version 3.4.3 (R Core Team, 2020) for the discrete and continuous characters, respectively, as listed in the ancestral state reconstruction section above. These functions estimate the phylogenetic signal, which is represented by  $\lambda$  for the discrete and continuous characters.  $\lambda$  values range from 0, which indicates characters are independent of the phylogeny, to 1 which indicates that along the given tree, the character states are correlated with species relationships as expected under a Brownian model of evolution (Harvey & Pagel, 1991). The log-likelihood of each character was calculated for a free model with characters optimized onto a tree with branch lengths derived from the three-gene Bayesian consensus tree, as well as with a model where  $\lambda$  is constrained to zero, which sets all branch lengths as equal. A  $\chi^2$  test was then used to calculate the degree of statistical significance (P-value) between the log-likelihoods of these two models,  $\log_L$  versus  $\log_{L0}$ , respectively. The function “fitDiscrete” was implemented for each character. The fit of each model (symmetrical [SYM], all rates different [ARD], and equal rates [ER]) was assessed using the Akaike Information Criterion (AIC). The highest AIC value was compared with the AIC for the remaining two models using a  $\chi^2$  test. Ultimately, the simplest model (the ER model) was used, as the differences in AIC values between the best fit and ER model were not statistically significant for each ancestral state reconstruction. Possible correlations between the characters were assessed using the comparative phylogenetics package *caper* (Orme et al., 2013) implemented in R version 3.4.3. We used the “comparative.data” function and fit an independent contrast regression model, which provides a P-value for each comparison (Table S5).

## 3 Results

### 3.1 GoFlag data sets

In order to test Fissidentaceae monophyly and locate the ingroup root, 11 outgroup samples were included in the analyses from four other families in the Dicranales M. Fleisch., including Dicranaceae (seven *Dicranum* Hedw. species), Ditrichaceae Limpr. (*Ceratodon purpureus* [Hedw.] Brid.), Leucobryaceae Schimp. (two *Leucobryum* Hampe species), and Grimmiaceae Arn. (*Racomitrium emersum* [Müll. Hal.] A. Jaeger). The eight taxa from the Dicranaceae and Ditrichaceae were targeted using the GoFlag 451 probe set, whereas the remainder of the taxa were targeted using the GoFlag 408 probe set, which completely overlaps with

the GoFlag 451 set (Breinholt et al., 2020, 2021). We submitted 43 samples representing 40 species in the genus *Fissidens* for sequencing with the GoFlag project (Table S1). Sequences from 418 loci were recovered. After removing reads with multiple variants, we recovered over 65% (273 out of 418) or more of the loci for all but two samples. These two samples, *Fissidens fasciculatus* Hornsch. (12 loci from 9.92 ng of DNA; MO-5377295, specimen collected from the field in 1997; SAMN27028511) and *Fissidens plumosus* Hornsch. (130 loci from 124.79 ng of DNA; MO-6363431, collected in 2000; SAMN27028512), were removed from the phylogenetic analyses. For the remaining *Fissidens* taxa 273 to 392 loci were recovered per sample. Fourteen of the 418 loci recovered contained sequences from fewer than 10 samples and thus these loci were removed from further analysis. The remaining 404 loci contained data from 41 *Fissidens* and 11 outgroup samples. The raw data are deposited in GenBank (Table S1).

Similar to the findings across a phylogenetically broader GoFlag data set (Breinholt et al., 2021), we did not find significant relationships between the amount of tissue sampled, the amount of DNA used in each sample (normalized to a maximum of 250 ng for the library preparation), or between specimen age and the number of loci generated (data not shown). As in Breinholt et al. (2021), there were some samples with very little extracted DNA that were successfully sequenced (e.g., *Fissidens porrectus* Mitt., 375 loci from 9.72 ng of DNA; MO-6495458, collected in 2012), potentially indicating that DNA quality rather than quantity may have a greater effect on the results using these methods.

After pruning the alignments to include only sites with data from 10 or more samples, the probe loci, which included only the exon regions, had alignments that were on average 184 bp long (range: 110–1014 bp); for loci in the full data set, which included conserved exon regions targeted by the sequencing probes and flanking intron regions, the alignments were on average 1220 bp (range 145–2532 bp). Each of these loci was then analyzed independently using ML and the resulting trees were used to construct the ASTRAL species tree. For the probe data set, the total aligned supermatrix is 74 441 nucleotides long with 10.0% missing data and 7.5% identical sites, whereas, for the full data set, the supermatrix is 493 051 nucleotides long with 31.4% missing data and 1.4% identical sites (data available on Dryad, doi:10.5061/dryad.gtht76hpg). The full data set is significantly longer and has a lower percentage of identical sites because it includes both the exons and the more variable intron regions. These supermatrices were used for the concatenated ML analyses and contained 94 partitions for the probe data set and 154 partitions for the full data set as determined using PartitionFinder2, with each partition containing single or multiple loci (Lanfear et al., 2016; Figs. S1, S2).

### 3.2 Three-gene data set

The concatenated matrix, comprising three loci, consisted of 1879 characters of which 10% were parsimony informative. The length, number of informative characters, and evolutionary model for each locus are reported in Table S3. All three loci were recovered for 77% of taxa in the final matrix,



and at least two loci were recovered for 98% of the sampled taxa. As expected for smaller data sets, when analyzed independently, each locus yielded a phylogenetic tree with diminished resolution compared to the phylogenetic analysis based on the concatenated matrix. However, the resolved topologies were largely congruent and there are no well-supported conflicts among the major clades (data available on Dryad, doi:10.5061/dryad.gtht76hpg). The raw data for three loci associated with all 111 samples are deposited in GenBank (Table S1).

### 3.3 GoFlag phylogenetic inferences

The concatenated ML analyses of the supermatrices for both the probe and full data set have high bootstrap support values (Figs. S1, S2) and are topologically congruent with the ASTRAL species tree (Fig. 1), with the exception that the relationships among the seven *Dicranum* species in the outgroup are not well-supported and differ between the analyses (Fig. 1 branches in orange). The bipartition analysis is summarized on the ASTRAL species tree using pie charts on each branch that indicate the percentage of gene trees for

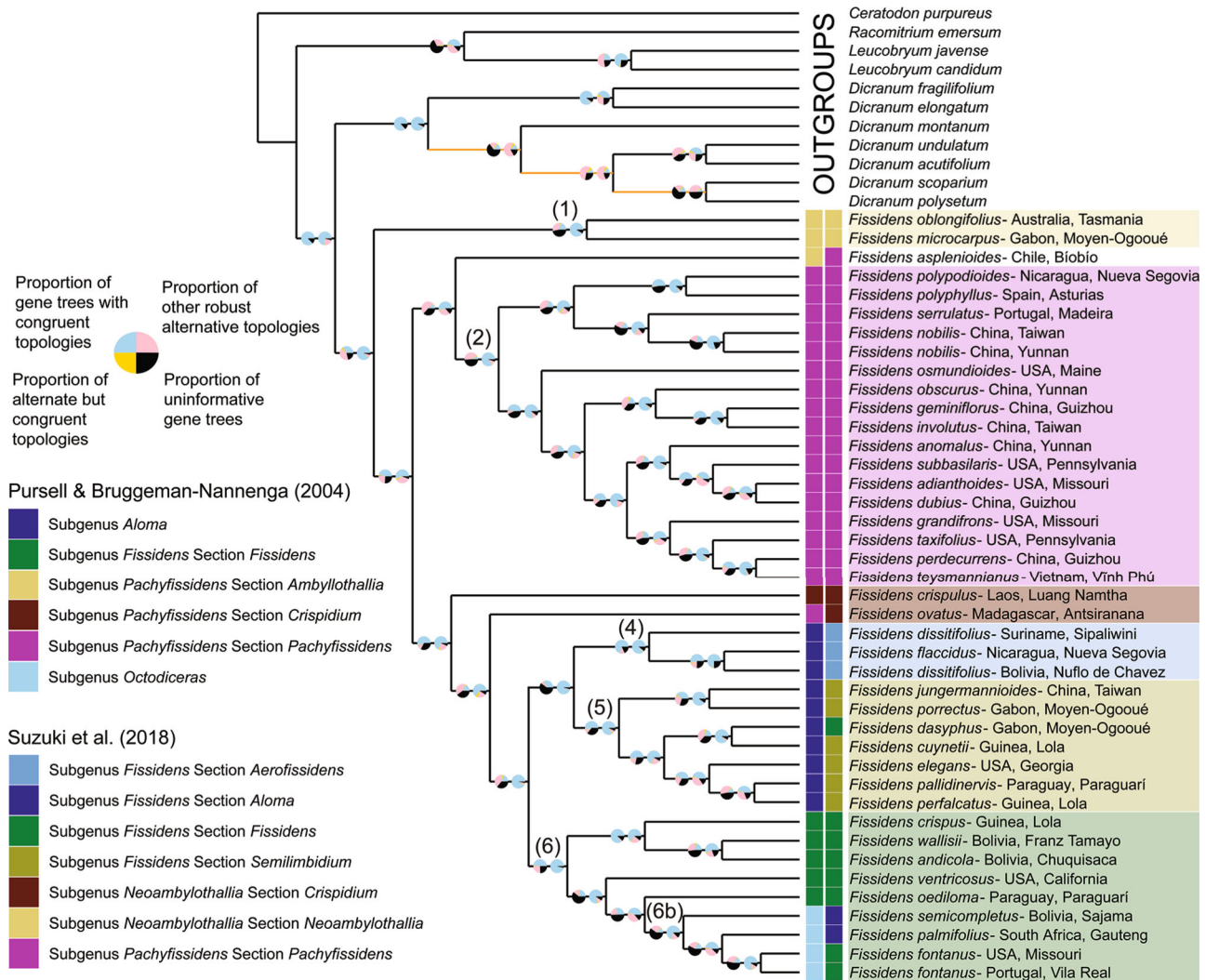


**Fig. 1.** Fissidentaceae phylogenomic inferences based on 404 loci targeted using next-generation sequencing technologies along with the GoFlag 451 and 408 loci probe sets (Breinholt et al., 2020). ASTRAL tree, which uses a multispecies coalescent approach (MSC) to infer a species tree from single locus gene trees. Pie diagrams on the branches (left pie is exons only [probe data set], right pie is exons and flanking regions [full data set]) represent the percentage of gene trees that are concordant with congruent topologies (blue), support the robust alternative topologies (pink), support all other alternative but congruent topologies (yellow), or are uninformative (black) for each bipartition. All branches between the *Fissidens* species are maximally supported using 1000 rapid bootstrap replicates in the concatenated analyses (see Figs. S1, S2), with the exception that some branches among *Dicranum* species are poorly supported (75% > bootstrap support > 25%) and/or have alternative topologies conflicting with the ASTRAL tree (branches in orange). Species were categorized into subgenera and sections according to the classification systems of Pursell & Bruggeman-Nannenga (2004; column of colored boxes on the left) and Suzuki et al. (2018; column of colored boxes on the right). Five of the six major clades numbered in the three-gene phylogeny (Fig. 2) are also represented and numbered here.

that bipartition with congruent topologies (blue), alternate but congruent topologies (yellow), other robust alternative topologies (pink), or are uninformative (black) with the pies indicating the support from the probe data set on the left and the full data set on the right (Fig. 1). The percentage of gene trees that are congruent (blue) is higher for the full data set in comparison to the probe at every node (Fig. 1). Branch support was also evaluated using the LPP (Figs. S3, S4) and multilocus bootstrap (MLBS; Figs. S5, S6) methods and results from these methods were congruent with the bipartition analysis. In all of these trees Fissidentaceae are strongly supported as monophyletic (Figs. 1, S1–S6). Well-supported clades with over 75% of the gene trees generated from the analysis of the full data set supporting congruent topologies are numbered on the phylogeny (right pies, blue wedge in Fig. 1).

### 3.4 Three-gene phylogenetic inferences

Phylogenetic inference based on the three-locus concatenated data set also yields a tree with strong support for Fissidentaceae monophyly (PP = 1; Fig. 2). *Fissidens* is split into two major lineages (comprising clades 1 and 2 versus clades 3–6 in Fig. 2) that are both well-supported (PP = 1 for both). Support for the divergence event producing these two groups is low (0.53), and hence their relative divergence is unresolved (Fig. 2). Corresponding branches for the well-supported clades are numbered in both the ASTRAL (Fig. 1) and BI trees (Fig. 2).

### 3.5 Classification systems

We mapped the classification systems of Pursell & Bruggeman-Nannenga (2004) and Suzuki et al. (2018) onto the ASTRAL species tree and the BI tree, respectively (Figs. 1, 2). Despite a number of well-supported clades, in the BI tree, each subgenus/section as defined by Pursell & Bruggeman-Nannenga (2004) and Suzuki et al. (2018) is polyphyletic (Fig. 2), whereas in the ASTRAL tree some of the subgenera and sections are supported as monophyletic (Fig. 1). Subgenus *Aloma* (Kindb.) Pursell & Brugg.-Nann. and subgenus *Octodiceras* (Brid.) Broth., as defined by Pursell & Bruggeman-Nannenga (2004), are both strongly supported as monophyletic (clades 4 + 5 and clade 6b in Fig. 1). For the classification system defined by Suzuki et al. (2018), subgenus *Neoambylohallia* Tad. Suzuki & Z. Iwats. section *Neoambylohallia* Tad. Suzuki (clade 1), subgenus *Pachyfissidens* (Müll. Hal.) Broth. section *Pachyfissidens* Müll. Hal. (clade 2), and subgenus *Fissidens* section *Aerofissidens* Müll. Hal. (clade 4) are supported as monophyletic (Fig. 1). Based on our sampling and molecular phylogenetic results, all other subgenera, and sections defined by these two classification systems are nonmonophyletic.

#### 3.5.1 Subgenus *Neoambylohallia*

Subgenus *Neoambylohallia* section *Neoambylohallia* as defined by Suzuki et al. (2018) is represented by two species in the ASTRAL tree (*Fissidens microcarpus* Mitt. and *F. oblongifolius* Hook. f. & Wilson) and they are strongly supported as monophyletic (Fig. 1). In our three-gene tree (Fig. 2), members of this section are polyphyletic. None of the five specimens of the pantropical species *F. oblongifolius* (type species of subgenus *Neoambylohallia*) are sisters to each other and members of other subgenera are nested in

this well-supported clade (Fig. 2, clade 1). However, the other two species of subgenus *Neoambylohallia* section *Neoambylohallia* (Suzuki et al., 2018) included in this analysis, *F. delicatulus* Ångstr. and *F. radicans* Mont., are both monophyletic and are closely related to three of the *F. oblongifolius* specimens, two from Australia and one from Puerto Rico (Fig. 2).

Subgenus *Pachyfissidens* section *Ambylohallia* Müll. Hal., as defined by Pursell & Bruggeman-Nannenga (2004), closely aligns with the Suzuki et al. (2018) concept of section *Neoambylohallia*, with the following exceptions: (i) *F. asplenoides* Hedw., is resolved with weak support sister to a clade that includes the majority of the other members of subgenus *Pachyfissidens* section *Pachyfissidens*, as defined by Suzuki et al. (2018; clade 2 in Figs. 1, 2); (ii) *F. fasciculatus* and *F. plumosus*, which are particularly challenging species to classify using morphology (Bruggeman-Nannenga & Berendsen, 1990), are sister to each other and closely related to section *Crispidium* Tad. Suzuki & Z. Iwats. (clade 3a in Fig. 2), and; (iii) *F. oblongifolius*, is polyphyletic, as previously mentioned (Fig. 2). All the other species nested in subgenus *Pachyfissidens* section *Ambylohallia* are classified by Pursell & Bruggeman-Nannenga (2004) as either subgenus *Aloma* or subgenus *Pachyfissidens* section *Pachyfissidens*.

#### 3.5.2 Subgenus *Pachyfissidens*

The majority of the species placed by Suzuki et al. (2018) into the subgenus *Pachyfissidens* section *Pachyfissidens* form a monophyletic lineage (clade 2 in Figs. 1, 2). In terms of species composition, this clade mostly aligns with the species that Pursell & Bruggeman-Nannenga (2004) placed into subgenus *Pachyfissidens* section *Pachyfissidens* based on morphology, with the following exceptions: (i) *F. ovatus* (Fig. 1) is more closely related to *F. crispulus* Brid., and this relationship aligns with the Suzuki et al. (2018) concept of section *Crispidium* and; (ii) single specimens of three diverse species (*F. anomalus* Mont., *F. nobilis* Griff., and *F. polypodioides* Hedw.) are located in a paraphyletic grade in which members of Suzuki et al. (2018) subgenus *Neoambylohallia* section *Neoambylohallia* are nested (Fig. 2). As mentioned earlier, *F. asplenoides* is weakly supported as sister to other members of subgenus *Pachyfissidens* section *Pachyfissidens* (clade 2 in Figs. 1, 2). Additional specimens that are classified into subgenus *Pachyfissidens* section *Pachyfissidens*, including specimens of *F. gymnogynus* Besch., *F. nobilis*, and *F. osmundioides* Hedw., do not have strongly supported relationships and fall outside the well-supported clades (those numbered in Fig. 2).

#### 3.5.3 Subgenus *Aloma*

All representative specimens of subgenus *Aloma*, as defined by Pursell & Bruggeman-Nannenga (2004), are strongly supported as monophyletic in our ASTRAL tree (clades 4 and 5 in Fig. 1). Subgenus *Aloma* is also moderately well-supported in our three-gene tree (clades 4 and 5 in Fig. 2), with the exception of eight specimens classified in this subgenus that are nested in other clades (Fig. 2; i.e., *F. dissitifolius* Sull., *F. exilis* Hedw., *F. pallidinervis* Mitt., and *F. pellucidus* Hornsch. nested in clade 1; *F. aoraiensis* H. Whittier & H.A. Mill. sister to clade 2; *F. serratus* Müll. Hal. sister to clades 4–6 and another specimen sister to clade 6; *F. zollingeri* Mont. in clade 6). In contrast, Suzuki et al. (2018) recognized *Aloma* in subgenus *Fissidens*. Section *Aloma*

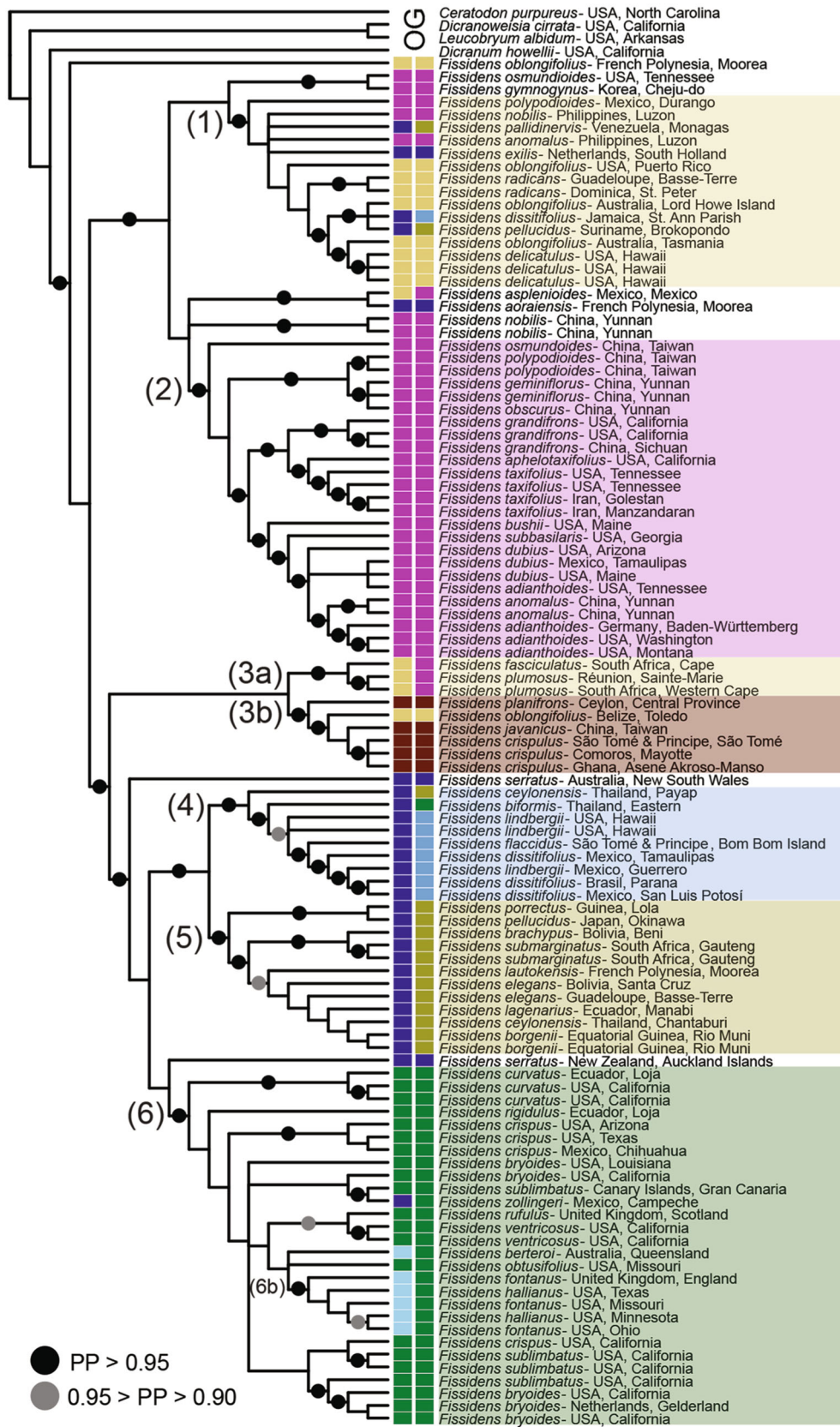


Fig. 2. Continued



(Suzuki et al., 2018) is represented by two samples in our ASTRAL tree [i.e., *F. semicompletus* Hedw. and *F. palmifolius* (P. Beauv.) Broth. in clade 6b Fig. 1]. In the three-gene tree (Fig. 2) none of the species classified by Suzuki et al. (2018) in subgenus *Fissidens* section *Aloma* (*F. aoraiensis*, *F. exilis*, *F. serratus*) are each other's closest relatives.

### 3.5.4 Subgenus *Fissidens*

Subgenus *Fissidens* as classified by Suzuki et al. (2018) contains five sections, including section *Aloma* (Table S2). Only section *Polypodiopsis* (Müll. Hal.) Paris is not included in our analyses. Subgenus *Fissidens* section *Aerofissidens* comprises three samples that form a well-supported clade in the ASTRAL tree (clade 4 in Fig. 1). In the three-gene tree the majority of the specimens in this section are also in a single lineage (clade 4 in Fig. 2), with the exception that one specimen of *F. dissitifolius* from Jamaica is nested in a clade containing mostly members of section *Neoambylohallia* (clade 1 in Fig. 2). All members of subgenus *Fissidens* section *Semilimbidium* in the ASTRAL phylogeny are located in a single clade (clade 5 in Fig. 1) but with one member of section *Fissidens* nested in this clade (*F. dasyphus* Welw. & Duby). In the three-gene tree, clade 5 (Fig. 2) is composed entirely of species from subgenus *Fissidens* section *Semilimbidium*. Three subgenus *Fissidens* section *Semilimbidium* specimens are located outside this clade (i.e., *F. pallidinervis* and *F. pellucidus* are in clade 1, and *F. ceylonensis* Dozy & Molk. is in clade 4).

The majority of the species in our phylogeny that were classified by Suzuki et al. (2018) as subgenus *Fissidens* section *Fissidens* are strongly supported as monophyletic in our trees (clade 6 in Figs. 1, 2). The exceptions are section *Fissidens* as defined by Suzuki & Iwatsuki (2007); as species, *F. biformis* is nested in clade 4 in the three-gene tree (Fig. 2), and in the ASTRAL tree, two members of section *Aloma* are nested in section *Fissidens* in clade 6 (Fig. 1) and section *Fissidens* species *F. daphysus* is nested among members of section *Semilimbidium* in clade 5. Subgenus *Fissidens*, as defined by Pursell & Bruggeman-Nannenga (2004), is paraphyletic in both trees with members of subgenus *Octodiceras* nested in clade 6 in both trees (clade 6b in Figs. 1, 2) and a single specimen of *F. zollingeri* nested in subgenus *Fissidens* in the three-gene tree (clade 6 in Fig. 2).

### 3.6 Phylogenetic signal and ancestral character state reconstructions

For the discrete characters, the proportional likelihood (PL) for each character state reconstructed for each node is represented by a pie chart (Figs. 3–5, S7–S9). In Dryad (doi:10.5061/dryad.gtht76hpg) a table with the likelihood

values associated with each state at each node, as well as a tree with each node numbered, is provided for reference. For the continuous characters, the likelihood reconstructions are displayed on the phylogenetic tree as a color gradation (Figs. 6, S10–S12).

#### 3.6.1 Morphological characters

The morphological characters axillary hyaline nodules, limbidium, costa, and peristome each exhibit statistically significant phylogenetic signals when tested on the three-gene phylogeny (Fig. 2; Table 1). The character sexual system has the strongest phylogenetic signal ( $\lambda = 0.99$ ). Peristome morphology is scored using two sets of definitions; one proposed by Bruggeman-Nannenga & Berendsen (1990), and the other by Suzuki & Iwatsuki (2007), abbreviated below as B-N&B1990 and S&I2007. The peristome morphology B-N&B1990 exhibits a slightly stronger phylogenetic signal ( $\lambda = 0.92$ ) than S&I2007 ( $\lambda = 0.83$ ). Among the morphological characters, peristome morphology S&I2007, has the lowest phylogenetic signal, although it is still statistically significant.

For the majority of the sampled species, axillary hyaline nodules are absent. The ML ancestral character reconstruction indicates with a high likelihood (PL > 0.75) that the ancestral condition for most major Fissidentaceae clades (1, 2, 4, 5, 6, 6b) and the backbone nodes are nodules absent (Fig. S7). The state is reconstructed as nodules absent with a lower likelihood (PL > 0.50) for clade 3a. Clade 3b is the only major clade where the ancestral character state is reconstructed as nodules prominent (PL > 0.90). Across the six major clades present in the tree, there are potentially 18 independent evolutionary transitions to nodules present, with seven transitions to nodules weak and 11 to nodules prominent, with no reversal to nodules absent reconstructed for this trait.

The ML reconstruction of costa anatomy predicts the most ancestral Fissidentaceae nodes as the *taxifolius*-type anatomy with a high likelihood (PL > 0.75; Fig. 3). This type is also reconstructed as the ancestral condition for clades 1, 2, and 3b with a very high likelihood in each case (Fig. 3). Clades 1 and 3b contain transitions to both the *bryoides*-, and *oblongifolius*-types, whereas all members of clade 2 share the *taxifolius*-type costa anatomy. The ancestral condition for clade 3a is reconstructed with very high likelihood (PL > 0.90) as the *oblongifolius*-type anatomy. The ancestral condition for clades 4, 5, 6, and the common ancestors of these three clades is reconstructed as the *bryoides*-type with a very high likelihood (PL > 0.90).

The ML reconstruction of the limbidium morphology indicates with a high likelihood (PL > 0.90; Fig. S8) that the ancestral condition for several of the major Fissidentaceae

**Fig. 2.** Fissidentaceae Bayesian inference majority rule consensus tree based on three loci (*trnA*, Wahrmond et al., 2008; *trnL-F*, Frey et al., 1999; *ITS2*, Stech & Frahm, 1999) generated using Sanger sequencing. Outgroup species (OG) are indicated at the top of the tree. Circles on the branches indicate the levels of posterior probability (PP) support with black circles indicating strong support (PP > 0.95) and gray circles indicating moderate support (0.95 > PP > 0.90). Species were categorized into subgenera and sections according to the classification systems of Pursell & Bruggeman-Nannenga (2004; column of colored boxes on the left) and Suzuki et al. (2018; column of colored boxes on the right) using the same color schemes as listed in Fig. 1. The major clades are indicated by numbers directly to the left of the branch with strong support for this clade, which correspond to the numbered branches in Fig. 1.

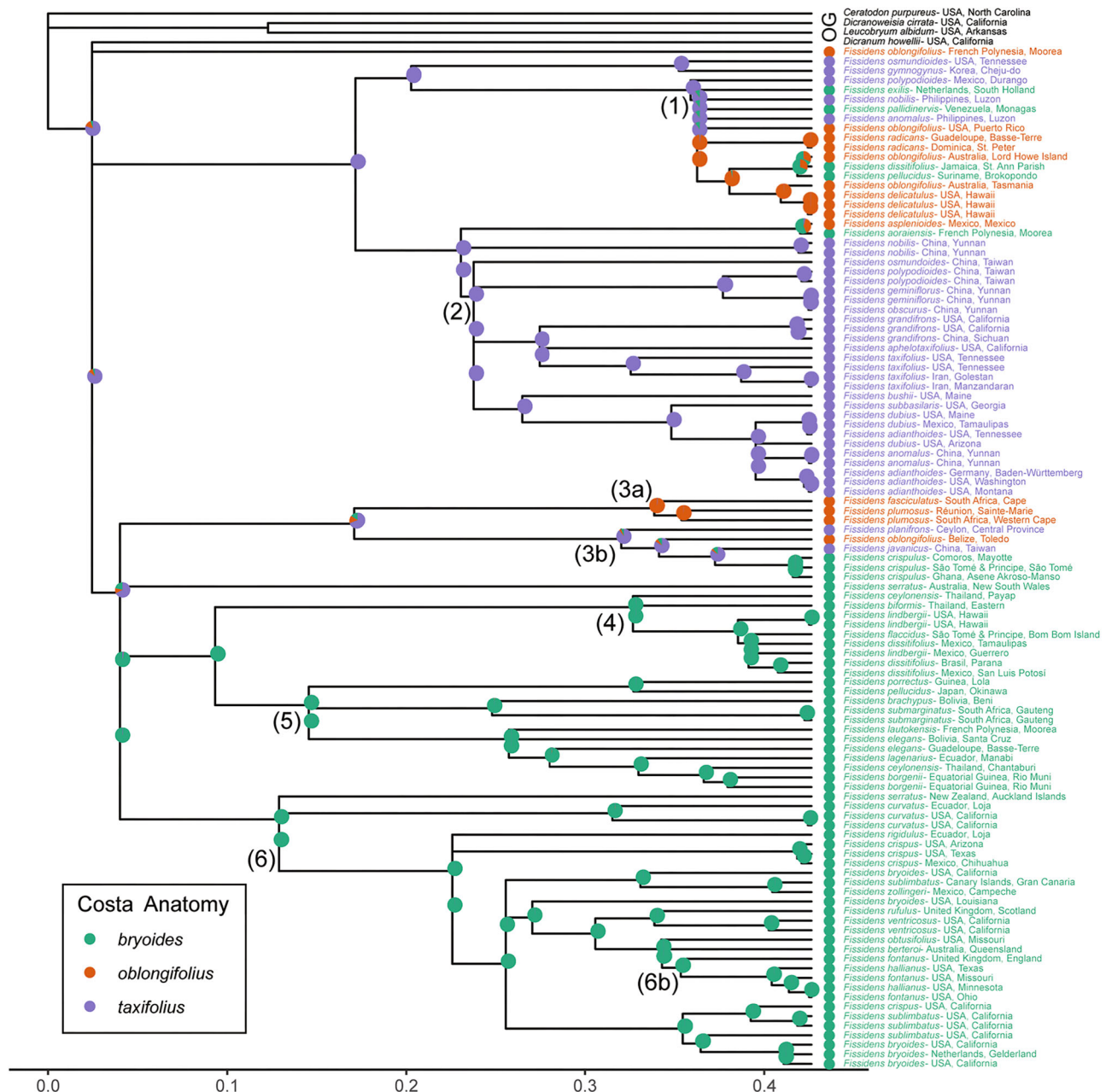


**Fig. 3.** Costa anatomy character states mapped onto an ultrametric version of the three-gene tree (Fig. 2) using maximum likelihood, with an equal rates model. The probability of the states at each node is shown as pie charts representing the proportional likelihood values for each character state. The scale bar represents the number of substitutions per site. The legend indicates the color associated with each character state. Species with missing data are in black text. *Fissidens crispulus* is mapped as having *bryoides*-costa anatomy, however, this species can also have leaves with a *taxifolius*-type on the same stem. The major clades, which correspond to the numbered branches in Fig. 2, are indicated on the tree.

clades (clades 1, 2, 3a, 3b) and the backbone nodes are elimbate. Within clade 1, there are a few transitions to partially to fully limbate leaves, whereas in clades 2, 3a, and 3b, all taxa sampled are elimbate. Transitions to partially or fully limbate conditions occur independently in clades 4, 5, and 6 (Fig. S8). Clade 5 contains taxa that are partially limbate to different degrees, including taxa that have one of the three middle character states. The vast

majority of the taxa in clades 4 and 6 are limbate on all regions of the lamina with a reversal to the elimbate condition in the aquatic taxa (e.g., *F. berteroi*, *F. fontanus*, and *F. hallianus*) in clade 6b.

The ML reconstructions for the ancestral Fissidentaceae nodes are ambiguous for peristome morphology (Fig. S9) as defined by B-N&B1990. Clade 1 contains taxa with four different peristome types and at least four transitions between

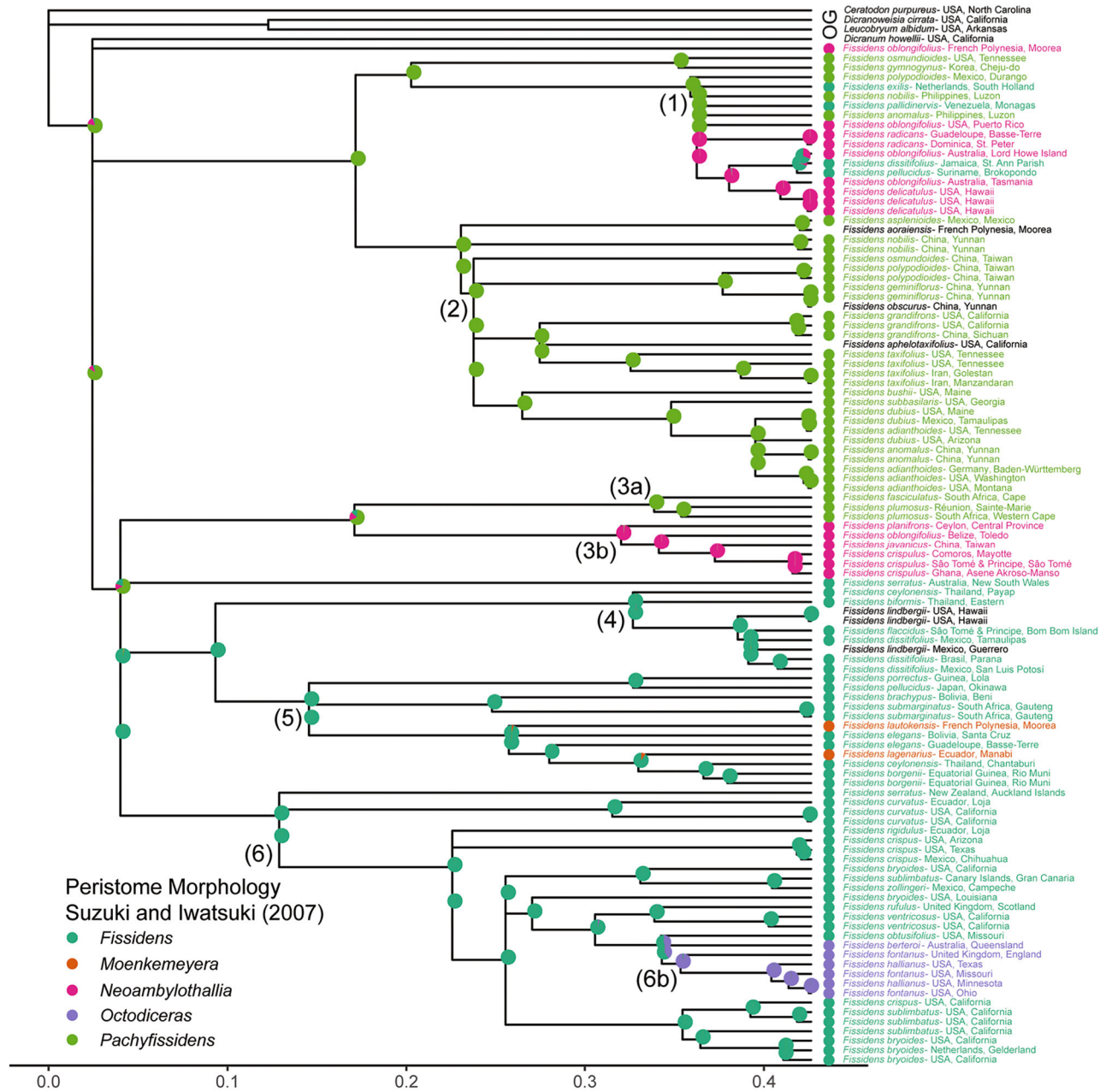


**Fig. 4.** Peristome morphology character states as defined by Suzuki & Iwatsuki (2007) mapped onto the three-gene Fissidentaceae Bayesian inference majority rule consensus tree using maximum likelihood, with an equal rates model. The probability of the states at each node is shown as pie charts representing the proportional likelihood values for each character state. The scale bar represents the number of substitutions per site. The legend indicates the color associated with each character state. Species with missing data are in black text. The major clades, which correspond to the numbered branches in Fig. 2, are indicated on the tree.

peristome types are reconstructed. The ancestral state for clade 2 is reconstructed as the *taxifolius*-type with a very high likelihood (PL > 0.90), with one transition to the *nobilis*-type peristome within this clade. The two members of clade 3a both share a *fasciculatus*-type peristome, whereas the ancestral condition for clade 3b was reconstructed as the *zippelianus*-type peristome with a very high likelihood (PL > 0.90). All taxa that could be scored for this character in clades 4 and 5 share the

*scariosus*-type, which was also reconstructed with a high likelihood (PL > 0.75) as the ancestral state for the common ancestor of clades 4, 5, and 6. The vast majority of the taxa in clade 6 have the *bryoides*-type peristome with a single transition to the *anomalus*-type in the aquatic taxa in clade 6b, section *Octodiceras*.

The ML reconstructions for the ancestral Fissidentaceae nodes are reconstructed as the *Pachyffissidens*-type for



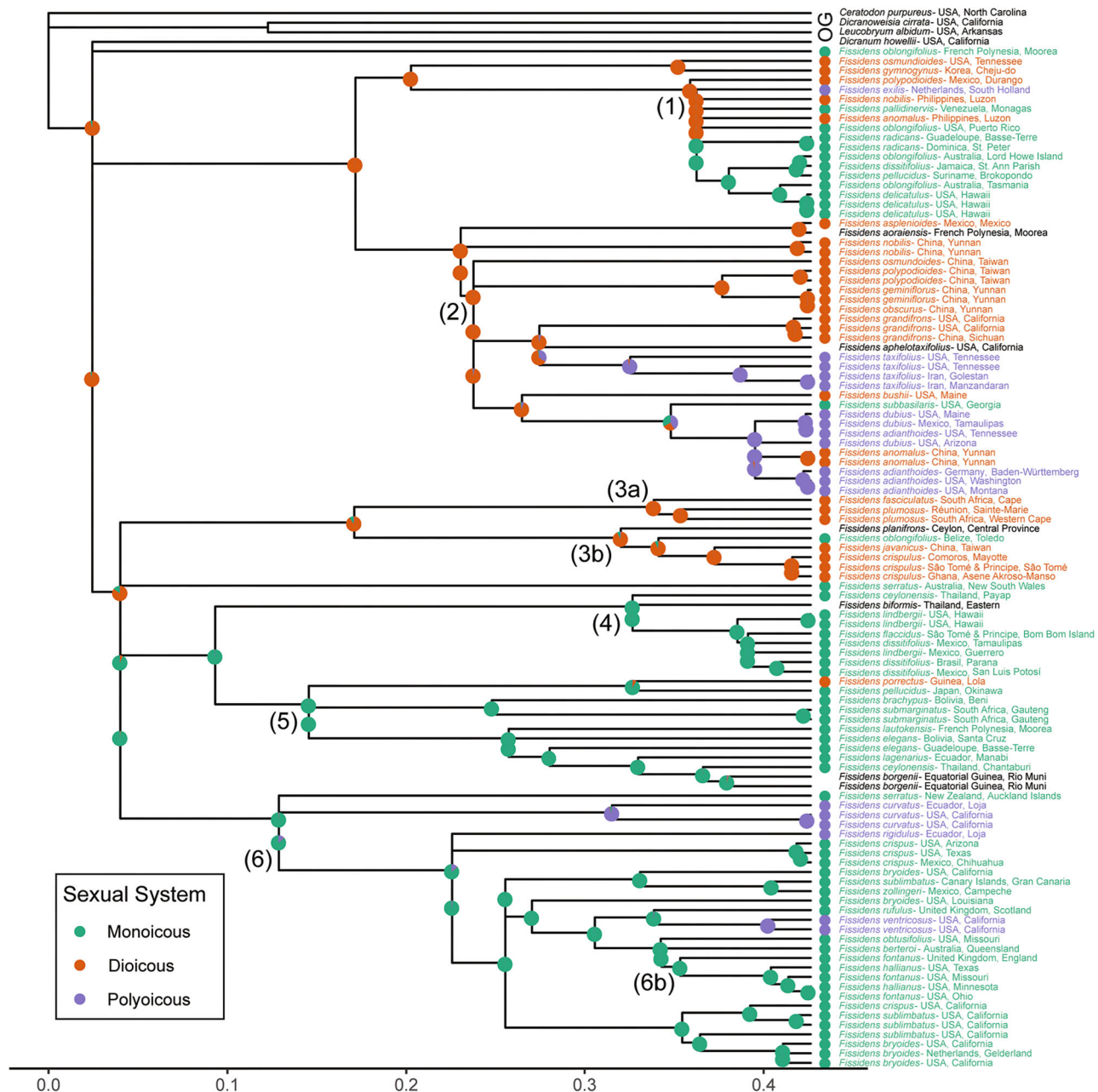


**Fig. 5.** Sexual system mapped onto the three-gene Fissidentaceae Bayesian inference majority rule consensus tree using maximum likelihood, with an equal rates model. The probability of the states at each node is shown as pie charts representing the proportional likelihood values for each character state. The scale bar represents the number of substitutions per site. The legend indicates the color associated with each character state. Species with missing data are in black text. The major clades, which correspond to the numbered branches in Fig. 2, are indicated on the tree.

peristome morphology (Fig. 4) as defined by S&I2007. The ancestral states for clades 1, 2, and 3a were reconstructed as the *Pachyfissidens*-type with a very high likelihood ( $PL > 0.90$ ). Clade 1 contains taxa with three different peristome types and three transitions between peristome types are reconstructed, whereas all members of clade 2 and 3a have the *Pachyfissidens*-type. The ancestral condition for clade 3b was reconstructed as the *Neoambylothallia*-type peristome with a very high likelihood ( $PL > 0.90$ ) with all members of this clade sharing this peristome type. The most recent common ancestor (MRCA)

of clades 4, 5, and 6 were all reconstructed as having the *Fissidens*-type with two transitions to the *Moenkemeyera*-type occurring in clade 5 and one transition to the *Octodicerias*-type in the aquatic taxa of clade 6b.

### 3.6.2 Sexual system

The character sexual system also exhibits a statistically significant phylogenetic signal ( $\lambda = 0.96$ , 1;  $P = 1.79e-12$ ). The ML reconstruction for the sexual system suggests that the ancestral nodes in Fissidentaceae were dioicous (exhibiting separate sexes), as were the ancestors for clades 1, 2, 3a, and 3b ( $PL > 0.90$ ; Fig. 5).

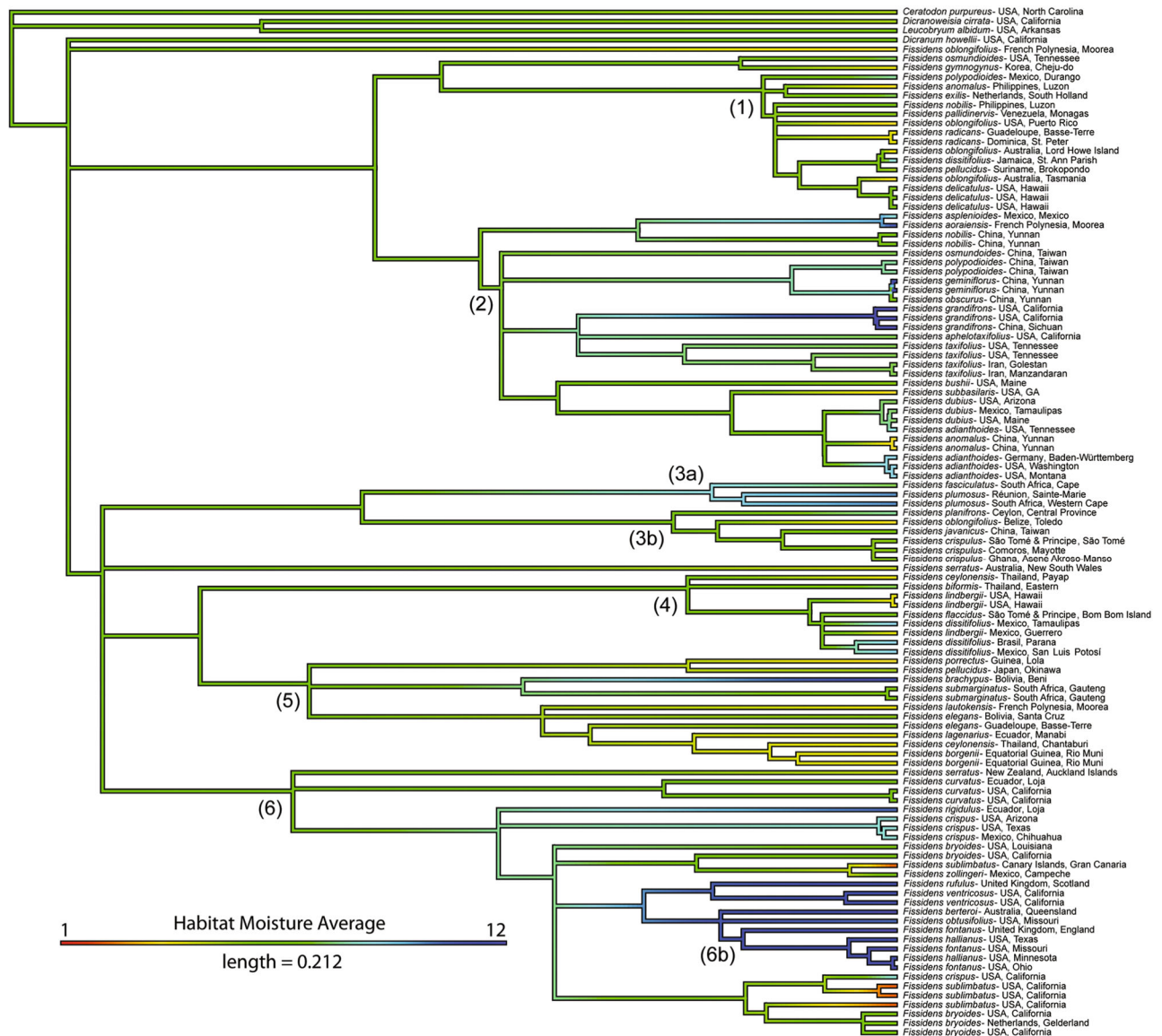


**Fig. 6.** Continuous character state mapping of the average habitat moisture, ranging from 1 (red) to 12 (blue), onto the three-gene Fissidentaceae Bayesian inference majority rule consensus tree using maximum likelihood. The length of the colored scale bar represents the number of substitutions per site. The major clades, which correspond to the numbered branches in Fig. 2, are indicated on the tree.

Clades 1, 2, and 3b include transitions to combined sexes with some taxa in clades 1 and 2 exhibiting both monoicy and dioicy, whereas the two taxa in clade 3a are both dioicous. Clades 4, 5, and 6 include taxa that are mainly monoicous, and hence monoicy is reconstructed as ancestral with a very high likelihood ( $PL > 0.90$ ) for all three of these clades. Clade 5 includes one transition back to dioicy and clade 6 includes two transitions to taxa that may have both sexual systems.

### 3.6.3 Habitat moisture

Minimum habitat moisture, average habitat moisture, maximum habitat moisture, and habitat moisture niche breadth were treated as continuous characters and each exhibits a statistically significant phylogenetic signal (Table 1). Among these characters, minimum habitat moisture has the highest  $\lambda$  value ( $\lambda = 0.81$ ) and maximum habitat moisture, the lowest

( $\lambda = 0.54$ ; Table 1). Intermediate moisture levels are reconstructed as ancestral across the backbone nodes for minimum habitat moisture (Ellenberg levels 5–6 “on moderately moist” to “moist soils” [Hill et al., 2007]; Fig. S10) and average habitat moisture and maximum habitat moisture (levels 7–8 “on constantly moist or damp, but not permanently waterlogged substrata” [Hill et al., 2007]; Figs. 6, S11). For average habitat moisture, there are at least seven independent transitions to very high moisture levels (10–12) across all the major Fissidentaceae clades, except for clade four (Fig. 6). While some taxa have shifted to a slightly lower average habitat moisture compared to the ancestral condition, there is only a transition to very low moisture levels (1–2) in *F. sublimbatum* Grout (clade 6; Fig. 6). The ancestral condition for the habitat moisture niche breadth for Fissidentaceae is three to four



(Fig. S12). The majority of species have a niche breadth of less than four. Across the phylogeny, there are transitions to both narrower (1–2) and wider (5–7) niche breadth in all major clades across the phylogeny, except for clade four which only contains transitions to narrower niche breadth (Fig. S12).

### 3.6.4 Character correlations

Preliminary analyses indicated that maximum habitat moisture is highly correlated with minimum moisture ( $adj R^2 = 0.59$ ,  $P = 2.20e-16$ ), average moisture ( $adj R^2 = 0.91$ ,  $P = 2.20e-16$ ), and niche breadth ( $adj R^2 = 0.42$ ,  $P = 2.47e-12$ ). Additionally, minimum moisture is highly correlated with average moisture ( $adj R^2 = 0.85$ ,  $P = 2.20e-16$ ). Thus moisture minimum and maximum were excluded from the correlation analyses (Fig. 7; Table S5). The two peristome morphology systems (Bruggeman-Nannenga & Berendsen, 1990; Suzuki & Iwatsuki, 2007) are also highly correlated ( $adj R^2 = 0.60$ ,  $P = 2.20e-16$ ). Preliminary analyses indicated a similar pattern for, but stronger relationships between, the S&I2007 system and other morphological features, and thus the peristome morphology system defined by B-N&B1990 was excluded from the correlation analyses (Fig. 7; Table S5). Across the remaining morphological characters, there are a number of statistically significant ( $P < 0.01$ ) correlations with low ( $\sim 0.25$ ) to high ( $> 0.70$ ) adjusted  $R^2$  values, indicating that the variance in the characters is explained by these relationships. Significant correlations were found between several of the morphological characters, and also between moisture and morphological characters (Fig. 7; Table S5).

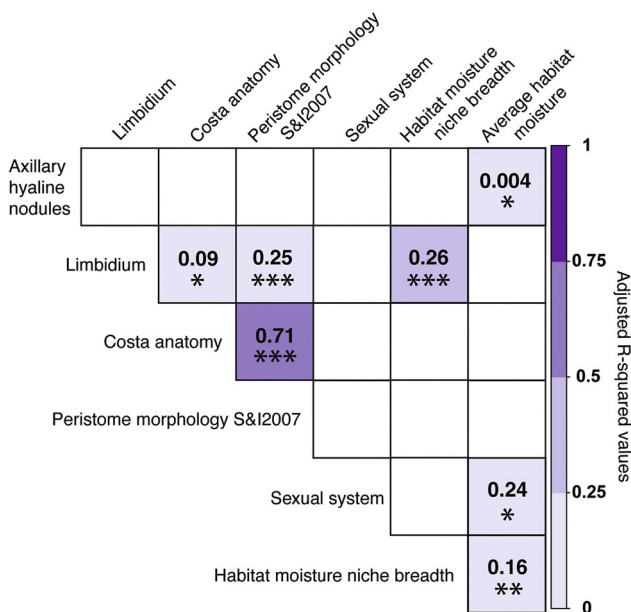


**Fig. 7.** Correlation matrix showing results between morphological characters and habitat traits. Correlations were assessed using *caper* implemented in R. We used the “comparative.data” function and fit an independent contrast regression model, which provided a  $P$ -value for each comparison. Adjusted  $R^2$  values are displayed for correlations with  $P$ -values less than 0.01.  $P$ -values are indicated by asterisks: \*  $< 0.01$ , \*\*  $< 0.0001$ , \*\*\*  $< 0.000001$ .

## 4 Discussion

Target-capture sequencing of single-copy nuclear loci has improved our understanding of relationships across flagellate plants in spite of confounding factors such as polyploidy, hybridization, and incomplete lineage sorting (e.g., Wickett et al., 2014; Qi et al., 2018). As has been highlighted in other studies (Liu et al., 2019; Medina et al., 2019; Breinholt et al., 2021; Thomas et al., 2021), we also find that including the noncoding regions flanking the targeted exons significantly strengthens our phylogenetic inferences (Fig. 1). Target enrichment further expands the utility of single-copy nuclear loci in phylogenetics by allowing for the generation of high-quality DNA sequences even from degraded DNA derived from older tissues, such as herbarium specimens. For this study, we relied exclusively on previously collected and identified specimens housed in several herbaria (ALTA, DAV, E, L, MO, TENN, and UC), thus saving both time and resources. Additionally, using herbarium specimens previously identified by taxonomic experts enables us to take full advantage of the time spent by researchers working on these collections. Target capture sequencing and analysis of collected data, utilized here, is just one of the ways that natural history collections are integral to modern scientific inquiry (e.g., Heberling & Isaacs, 2017; Viruel et al., 2019; Hale et al., 2020).

Each morphological character scored in the present study exhibits a significant phylogenetic signal (Table 1), suggesting that these are synapomorphic for some clades and generally informative for understanding the evolution of Fissidens. These morphological features have long been used in taxonomic classifications of Fissidentaceae species (Potier de la Varde, 1931; Norkett, 1969; Bruggeman-Nannenga, 1974, 1978; Iwatsuki, 1985; Pursell, 1987; Pursell et al., 1988; Bruggeman-Nannenga & Berendsen, 1990; Pursell & Bruggeman-Nannenga, 2004; Suzuki & Iwatsuki, 2007) and our findings reinforce the importance of these features for understanding Fissidentaceae evolution and as classification markers. Exploring relationships between morphological evolution and ecology across mosses is also a long-standing area of research (e.g., Proctor, 1979; Schofield, 1981) that continues to be explored (e.g., Hedenäs, 2001; Vanderpoorten et al., 2002; Huttunen et al., 2012; Rose et al., 2016). Despite the proposal that ecological factors may impact the gametophyte phase more than the sporophyte phase in bryophytes (Stanton & Reeb, 2016), we found correlations between habitat moisture characters and both gametophyte and sporophyte features in *Fissidens*. These correlations suggest that these features may be adaptive (Huttunen et al., 2018). Accordingly, the morphological characters described here warrant further exploration in both the context of taxonomy and functional evolution.

### 4.1 Peristome morphology

Peristome teeth generally regulate the opening and closing of sporophyte capsules and fully formed peristome teeth are critical for spore dispersal by wind (Vitt, 1981). Reductions in peristome morphology can occur when species transition from terrestrial to aquatic habitats, particularly when the spores are no longer wind-dispersed and instead rely on water dispersal, or from terrestrial to epiphytic habitats, where spore dispersal is then facilitated by the height of the

**Table 1** Phylogenetic signal ( $\lambda$  value) for each morphological character (axillary hyaline nodule, costa, limbidium, peristome morphology, sexual system, and habitat moisture, the latter including minimum, average, maximum, and niche breadth), as reconstructed on the three-gene Bayesian tree for *Fissidens*.

Discrete characters	$\lambda$	$\log_L$	$\log_{L0}$	P-value (log-likelihood from “fitDiscrete”)
Axillary hyaline nodules	0.85	−98.16	−115.21	4.44e−16*
Costa anatomy	0.94	66.79	147.10	1.02e−24*
Limbidium	0.93	−91.58	−153.21	8.61e−38*
Peristome morphology (Bruggeman-Nannenga & Berendsen, 1990)	0.92	−136.10	−237.03	2.91e−30*
Peristome morphology (Suzuki & Iwatsuki, 2007)	0.83	−104.57	−187.34	1.93e−22*
Sexual system	0.99	−82.23	−144.91	1.79e−12*
Continuous characters	$\lambda$	$\log_L$	$\log_{L0}$	P-value (log-likelihood from “fitContinuous”)
Habitat moisture minimum	0.81	−312.95	−271.59	<1.00e−30*
Habitat moisture average	0.74	−313.80	−270.31	<1.00e−30*
Habitat moisture maximum	0.54	−323.39	−278.62	<1.00e−30*
Habitat moisture niche breadth	0.69	−216.16	−242.50	3.93e−13*

The level of statistical significance, based on comparing AIC (Akaike information criterion) values with either the estimated branch lengths versus branch lengths set to be equal, is given as a P-value with values less than 0.01 marked with an asterisk (\*) to indicate statistical significance.

mosses above the ground (Hedenäs, 2001, 2012; Huttunen, 2004; Olsson et al., 2009; Pokorný et al., 2012; Medina & Esté Banez, 2014). These observations suggest that these morphological shifts result from natural selection.

Vitt (1981) hypothesized that more complex peristomes are associated with mesic habitats, while reduced peristomes are associated with aquatic habitats. Complex peristome morphology and ornamentation may provide larger surface areas and more diverse locations for spores to lodge, thus enhancing spore dispersal for species with arthrodontous peristomes (Kungu et al., 2003; Gallenmüller et al., 2018). In *Fissidens*, Beever (1995) suggested that the shorter more irregular peristome teeth characterizing the *anomalous*-type may be the result of relaxed selection on species that are dispersing spores aequatically, whereas in terrestrial habitats complex peristome morphology is maintained through selection to facilitate wind dispersal. In line with the hypothesis of Beever (1995), species classified by Pursell & Bruggeman-Nannenga (2004) in subgenus *Octodiceras* (clade 6b in Figs. 1, 2), which is composed of taxa that are normally fully submerged aquatics (Ellenberg moisture value = 12; Figs. 6, S10, S11), have either *anomalous* (sensu Bruggeman-Nannenga & Berendsen, 1990; Fig. S9) or *Octodiceras*-type (sensu Suzuki & Iwatsuki, 2007; Fig. 4) peristomes. However, we do not find a significant correlation between peristome morphology and habitat moisture (Table S5). Outside subgenus *Octodiceras*, there are other *Fissidens* species that have also transitioned to aquatic habitats (e.g., *F. geminiflorus* Dozy & Molk., *F. grandifrons* Brid. in Fig. 6), but their peristome morphology is not necessarily reduced (Figs. 4, S9). Thus, in these taxa, there may be a selection for maintaining a peristome, even in aquatic habitats.

Sporophyte and gametophyte morphology have been noted to evolve independently both across *Fissidens* species (Suzuki et al., 2018) and in other mosses (Rohrer, 1988; Shaw & Beer, 1997; Pokorný et al., 2012). While this is also the case for several

of the characters analyzed in this study, we also found significant correlations between several gametophyte and sporophyte characters (Fig. 7; Table S5). We found that peristome morphology S&I2007 is significantly correlated with costa anatomy. This relationship was previously recognized by Bruggeman-Nannenga (1990) and Stone (1990) for *Fissidens* and is confirmed here (Fig. 7; Table S5). *Fissidens* species with *taxifolius* costa anatomy are more likely to have *Pachyfissidens*-type peristome morphology (Suzuki & Iwatsuki, 2007; Figs. 3, 4), whereas species with *bryoides* costa anatomy are more likely to have the *Fissidens/Octodiceras*-type (Suzuki & Iwatsuki, 2007). Peristome morphology is also correlated with limbidium morphology (Fig. 7; Table S5). Our results suggest that *Fissidens* species that are limbate on all lamina are most likely to have *Fissidens*-type (Suzuki & Iwatsuki, 2007) peristome morphology, whereas elimbate species have a wider array of peristome morphologies (Figs. 4, S8). Correlations between gametophyte and sporophyte morphology could point to these structures being under similar selection pressures since these two phases are connected throughout the lifespan of the sporophyte and thus occupy the same physical space. Alternatively, these correlations could be the result of genetic linkage or pleiotropy, since both phases are built by the same underlying genetics and differ only in terms of expression. A common feature among these morphological characters is that they are determined by differences in cell size and wall thickness; thus, the genes regulating these cellular aspects, such as PpVNS (Xu et al., 2014), could potentially influence their development. However, a functional explanation for correlations between these gametophyte and sporophyte structural characters has yet to be explored.

#### 4.2 Axillary hyaline nodules

Prominent nodules have been used as a diagnostic feature for section *Crispidium* (Pursell & Bruggeman-Nannenga,

2004; Suzuki & Iwatsuki, 2007) and were reconstructed by Suzuki et al. (2018) as synapomorphic for this clade. However, nodules ranging from weak to prominent are found in species outside the section *Crispidium* (Iwatsuki, 1977; Iwatsuki & Suzuki, 1977). Our reconstruction found that taxa with weak or prominent nodules are present in all six of the clades recovered during this analysis (Figs. 1, 2) and have potentially independently evolved in each clade (Fig. S7). Thus the presence of prominent axillary hyaline nodules is not unique to section *Crispidium* and nodule evolution is a labile feature that varies across the *Fissidens* phylogeny.

#### 4.3 Limbodium

Most taxa sampled in our phylogeny are at one of the two ends of the spectrum for limbodium morphology, either with a limbodium present on all regions of the lamina or with lamina that is elimbate (Fig. S8). Limbodium absent is reconstructed as the ancestral condition for Fissidentaceae in both Suzuki et al. (2018) and our study. Independent transitions to limbodium present were reconstructed in both of these studies. The extent of the limbodium around the lamina edge varies across species, as does the size, shape, and number of files of cells that compose the limbodium. Reversals to the elimbate condition were also reconstructed by Suzuki et al. (2018) and in our study (Fig. S8). It is well known that aquatic taxa lack differentiated lamina borders (Glime & Vitt, 1984) and Fissidentaceae includes many taxa that occupy aquatic habitats. Our reconstruction suggests that the obligately aquatic taxa in clade 6b (subgenus *Octodiceras*) represent an evolutionary reduction in limbodium morphology from ancestors with fully limbate lamina (Fig. S8). In contrast, Pokorny et al. (2012) found that models lacking (or with a low probability for) reversals were better for reconstructing limbodium evolution in Hookeriales. However, this result is potentially explained by their sampling, which focused on epiphytes and did not include species from aquatic habitats.

Functionally the limbodium may provide structural support to the moss phyllid (Lowell, 1998) and may also be involved in water storage (Daniels, 1998) and/or movement (Glime, 2017). However, these functional roles have not been explored experimentally. If the limbodium does play a role in water storage/movement we would predict that this structure would be functionally advantageous for species living in drier habitats. In *Fissidens*, we found a significant positive correlation between limbodium morphology and niche breadth (Fig. 7; Table S5), indicating that species with a limbodium present on all regions of the lamina are associated with a wider niche breadth. One potential interpretation is that a more extensive limbodium enables these species to survive across a wider variety of habitats and thus to be more flexible in their niche choice. These taxa also may have the developmental plasticity to produce a limbodium in dry conditions and not under more moist conditions, as has been observed in *F. adianthoides* Hedw. (Zastrow, 1934).

#### 4.4 Costa anatomy

Costa anatomy in the region of the vaginant lamina has been characterized in *Fissidens* by a number of authors, including Bruggeman-Nannenga (1974), Iwatsuki & Suzuki (1982), Pursell (1966, 1987, 1989), Pursell & Reese (1985), Stone (1987), Pursell et al. (1988), Bruggeman-Nannenga (1990),

Stone (1990), and Suzuki et al. (2018). Many of these studies used morphological differences in costa anatomy to define *Fissidens* subgenera and sections. Our reconstruction determined the ancestral node has a *taxifolius*-type costa (Fig. 3), which is characterized by two lateral sterid bands, four or more peripheral guide cells, and one to several large central cells. In contrast, Suzuki et al. (2018) inferred that the ancestral node had a *bryoides*-type costa, which is characterized by two lateral sterid bands, two peripheral guide cells, and generally one large central cell. This difference is potentially driven by the fact that the vast majority of the species included in the Suzuki et al. (2018) study have a *bryoides*-type costa and/or that their sampling was concentrated on Asia, in comparison to our global sampling. However, our reconstruction of costa anatomy demonstrates morphological conservation across the phylogeny with few transitions in character states across the tree (Fig. 3).

#### 4.5 Habitat moisture

Overall, habitat moisture levels are variable across *Fissidens* species, as might be expected for a diverse cosmopolitan genus (Figs. 6, S10, S11). However, all of the moisture-related traits exhibit significant phylogenetic signals (Table 1) indicating that species with a similar fundamental niche are more closely related (Losos, 2008). As the moisture character with the highest phylogenetic signal, transitions among habitat moisture minimum levels are also inferred to be infrequent (Fig. S10). The vast majority of *Fissidens* species occupy high moisture environments, and desiccation tolerance in *Fissidens*, here defined as a habitat moisture minimum of less than three, has evolved only in *F. sublimbatus*, which is reconstructed as polyphyletic in our analyses. While the ancestral condition for mosses is the presence of desiccation tolerance (Proctor et al., 2007), the ability of individual species to tolerate desiccation is variable across mosses (Stark, 2017). The ability to tolerate desiccation events necessitates a complex suite of morphological and physiological characteristics (Gaff & Oliver, 2013), and although re-evolving desiccation tolerance is possible (Illing et al., 2005; Oliver et al., 2005), this does not appear to be the case in *Fissidens*.

In contrast, *Fissidens* species exhibit more frequent shifts in habitat moisture niche breadth. The majority of these shifts occur from wider to narrower niches (Fig. S12). These contractions point toward the evolution of habitat specialization across *Fissidens*. In our study, taxa have the potential to range from specialists (niche breadth level = 1) to generalists (level = 12). However, the highest level of generalization for the *Fissidens* species included in this study is a habitat moisture niche breadth of seven (i.e., *F. dissitifolius*). Taxa that can tolerate a broader range of habitats may have lower levels of peak performance across these diverse niches (Sexton et al., 2017), whereas *Fissidens* taxa that are specialized for a narrower range of habitat moisture levels may have higher fitness in these habitats, which would be consistent with a trade-off in terms of tolerance breadth and peak performance levels (Lynch & Gabriel, 1987). Thus, *Fissidens* represents an interesting opportunity for testing performance within and outside observed niche breadth for species in which a narrow niche

breadth may suggest constrained evolution or stabilizing selection (Hansen, 1997; Johnson et al., 2014).

#### 4.6 Sexual system

The sexual system has been used as a defining feature for a number of *Fissidentaceae* subgenera and sections (Iwatsuki & Suzuki, 1982; Nyholm, 1986; Suzuki et al., 2018), and indeed we find that the sexual system has a strong phylogenetic signal (Table 1). We tested three models of character evolution for the sexual system; there was not a significant difference between the models, and thus directional evolution was not detected for the sexual system in *Fissidentaceae* mosses (Table S4). Bryophyte studies commonly reconstruct sexual systems using two character states: monoicous/combined sexes or dioicous/separate sexes (Crawford et al., 2009; McDaniel et al., 2013; Villarreal & Renner, 2013). However, in our study, we found disagreement in the literature with instances of different sexual systems reported from two regions of the world for a given species, and also observations from the same region of both monoicous and dioicous individuals and/or populations. Unfortunately, this disagreement could not be resolved using herbarium material because gametangia are often lacking for *Fissidens* specimens. This represents a gap in our knowledge of *Fissidens* life history. Documentation of sexual systems from multiple populations per species across different regions of the world would help us to capture potential intraspecific variation in this character.

Intraspecific variation in the sexual system in mosses has been attributed to variation in the ploidy level. Jesson et al. (2010) observed intraspecific variation in the sexual system associated with the ploidy level in *Atrichum undulatum* (Hedw.) P. Beauv.: monoicous individuals were always diploid or triploid. Monoicy comes with the potential advantage of higher rates of reproductive success (Smith, 1978; During, 2007; Dos Santos et al., 2020). Of the almost 50 *Fissidens* species included in Fritsch (1991), approximately 30% of these taxa have multiple ploidy levels reported for a single species. This could explain the infraspecific variation in the sexual system seen in our study, although this hypothesis remains untested. Ongoing explorations of genome size (Bainard et al., 2020) and polyploidy (Patel et al., 2021) will continue to enhance our ability to correlate genomic evolution with other aspects of life history and morphology in mosses.

Theory predicts that selection on morphological features involved in dispersal should differ between dioicous and monoicous species (Wilson & Harder, 2003). Selection for higher dispersal is predicted in dioicous species because dispersal increases the likelihood that gametophytes with opposite sexes will be located closer together, thus increasing the likelihood of sexual reproduction. Previous studies found that dioicous species were more likely to have smaller spores, which are more dispersible, compared to monoicous species (During, 2007; Crawford et al., 2009). While peristome teeth have long been known to play a role in spore dispersal (Goebel, 1905), we do not find a correlation between the sexual system and peristome morphology (Fig. 7; Table S5). However, the relationship between particular peristome structures/ornamentations and dispersal ability warrants further exploration. Future experimental

studies testing for structure–function relationships in moss sporophytes will be crucial in advancing our understanding of the connections between morphological evolution and life history.

We did find that the sexual system is weakly correlated with habitat moisture average (Fig. 7). This positive correlation indicates that both dioicous and polyoicous species are weakly correlated with higher moisture habitats (Table S5). Moisture is crucial for fertilization in mosses (Muggoch & Walton, 1942), and hence dioicous moss species, which require their swimming sperm to move between separate male and female gametophytes for syngamy to occur (McQueen, 1985; Crum, 2001), would be predicted to benefit more from moist environments compared to monoicous species. In low moisture environments, a greater ability for sperm to survive desiccation (Shortlidge et al., 2012) could be more beneficial to dioicous species in comparison to monoicous species.

#### 4.7 *Fissidentaceae* classification

Subgeneric and section delimitations in *Fissidens* vary across treatments and these concepts have changed over time (Müller, 1848, 1851, 1900; Brotherus, 1901, 1924; Potier de la Varde, 1931; Norkett, 1969; Bruggeman-Nannenga, 1974, 1978; Iwatsuki, 1985; Pursell, 1987; Pursell et al., 1988; Bruggeman-Nannenga & Berendsen, 1990; Pursell & Bruggeman-Nannenga, 2004; Suzuki & Iwatsuki, 2007; Suzuki et al., 2018). Pursell (1994) highlights intraspecific morphological variation as a particular challenge to taxonomic classification in *Fissidens*, but there are other challenges too, including inconsistently applied species concepts across taxonomic treatments and broadly distributed species. Despite a number of well-supported clades in the three-gene tree, each subgenus, and section as defined by Pursell & Bruggeman-Nannenga (2004) and Suzuki et al. (2018), is polyphyletic (Fig. 2). This tree is based on a limited number of loci; thus, some of these relationships may gain resolution and higher support with additional data. In contrast, the ASTRAL tree is based on hundreds of genes, and subgenera/sections from each classification system are supported as monophyletic (Fig. 1). In order to establish a revised classification system, specimens of the type species for each of the subgenera/sections should be included to anchor the nomenclature to the understanding of phylogenetic relationships.

## 5 Conclusions

The morphological features traditionally used to define subgenera and sections in *Fissidens* have high levels of phylogenetic signals. Additionally, some of these characteristics are correlated, both with each other and with aspects of the habitat moisture level. Some morphological features, such as axillary hyaline nodules and limbidium, are evolutionarily labile with multiple transitions across the *Fissidentaceae* phylogeny. On the other hand, costa anatomy and peristome morphology have fewer character state transitions and define well-supported clades. Correlations between gametophyte and sporophyte morphological characters could reflect the evolutionary recruitment of genetic

networks from the gametophyte to the sporophyte phase (Niklas & Kutschera, 2009) or vice versa, and their continued developmental linkage. In contrast, correlations between morphological characters and moisture levels may be the result of adaptive evolution to particular habitats (Huttunen et al., 2012). An ongoing exploration of the relationships between morphology and habitat will enable us to continue to expand our understanding of morphological evolution in mosses.

## Acknowledgements

Thanks to Victoria Beard, Nathan Kingsley, Daniel Kirk, and Sarah Wike at the University of Tennessee and Eunice Magat and Kristina Khuu at the University of California, Davis for generating sequence data for the three gene phylogenetic analyses. We also appreciate John Brinda (MO) for his thoughtful discussions on nomenclatural challenges, Margaret Oliver (TENN) for her assistance in compiling the herbarium specimen data, the University of Tennessee Genomics Core for assistance with sequencing as well as the editor and two reviewers for providing thoughtful comments that improved the manuscript. We appreciate the work of all of the researchers who collected and determined the specimens we used in this study. We also gratefully appreciate the following herbaria for allowing us to sample material from their specimens, including ALTA, DAV, E, L, MO, TENN, and UC. This work was supported in part by a Katherine Esau Postdoctoral Fellowship at the University of California, Davis to J.M.B. We appreciate the U.S. National Science Foundation for its support of the GoFlag Consortium (DEB-1541506).

## References

- Bainard JD, Newmaster SG, Budke JM. 2020. Genome size and endopolyploidy evolution across the moss phylogeny. *Annals of Botany* 125: 543–555.
- Beever JE. 1995. Studies of *Fissidens* (Bryophyta: Musci) in New Zealand: *F. strictus* Hook. f. & Wils. and *F. berteroi* (Mont.) C. Muell., with a discussion of aquatic adaptations. *New Zealand Journal of Botany* 33: 293–299.
- Bonfim Santos M, Fedosov V, Hartman T, Fedorova A, Siebel H, Stech M. 2021. Phylogenetic inferences reveal deep polyphyly of Aongstroemiaceae and Dicranellaceae within the haplolepidous mosses (Dicranidae, Bryophyta). *Taxon* 70: 246–262.
- Breinholt JW, Earl C, Lemmon AR, Lemmon EM, Xiao L, Kawahara AY. 2018. Resolving relationships among the megadiverse butterflies and moths with a novel pipeline for anchored phylogenomics. *Systematic Biology* 67: 78–93.
- Breinholt JW, Carey SB, Tiley GP, Davis EC, Endara L, McDaniel SF, Neves LG. 2020. Target enrichment probe set for resolving the flagellate land plant tree of life. Dryad Dataset. <https://doi.org/10.5061/dryad.7pvmcqvqg>
- Breinholt JW, Carey SB, Tiley GP, Davis EC, Endara L, McDaniel SF, Neves LG, Sessa EB, Konrat M, von Chantanaorrapint S, Fawcett S, Ickert-Bond SM, Labiak PH, Larraín J, Lehnert M, Lewis LR, Nagalingum NS, Patel N, Rensing SA, Burleigh JG. 2021. A target enrichment probe set for resolving the flagellate land plant tree of life. *Applications in Plant Sciences* 9: e11406.
- Brotherus VF. 1901. Fissidentaceae. In: Engler HGA, Prantl KAE eds. *Natürlichen Pflanzenfamilien*. Leipzig, Germany: Engelmann. 1: 143–155.
- Brotherus VF. 1924. Fissidentaceae. In: Engler HGA, Prantl KAE eds. *Natürlichen Pflanzenfamilien*. Leipzig, Germany: Engelmann. 2: 143–155.
- Bruggeman-Nannenga MA. 1974. On the characterization and the taxonomic status of the group of *Fissidens* species known as Pachyfissidens. *Mededelingen van Het Botanisch Museum En Herbarium van de Rijksuniversiteit Te Utrecht* 404: 141–148.
- Bruggeman-Nannenga MA. 1978. Notes on *Fissidens* parts 1 and 2. *Proceedings of the Koninklijke Nederlandse Akademie van Wetenschappen Series C Biological and Medical Sciences* 81: 387–402.
- Bruggeman-Nannenga MA. 1990. On the anatomy of the costa in *Fissidens*. *Bryophyte Diversity and Evolution* 3: 37–44.
- Bruggeman-Nannenga MA, Berendsen W. 1990. On the peristome types found in the Fissidentaceae and their importance for the classifications. *Journal Hattori Botanical Laboratory* 68: 193–234.
- Buck WR. 1994. A new attempt at understanding the Meteoriaceae. *Journal Hattori Botanical Laboratory* 75: 51–72.
- Chamberlin MA. 1980. *The morphology and development of the gametophytes of Fissidens and Bryoxiphium (Bryophyta)*. M.Sc. Thesis. Carbondale: Southern Illinois University.
- Cox CJ. 2018. Land plant molecular phylogenetics: a review with comments on evaluating incongruence among phylogenies. *Critical Reviews in Plant Sciences* 37: 113–127.
- Cox CJ, Li B, Foster PG, Embley TM, Civián P. 2014. Conflicting phylogenies for early land plants are caused by composition biases among synonymous substitutions. *Systematic Biology* 63: 272–279.
- Crawford M, Jesson LLK, Garnock-Jones PPJ. 2009. Correlated evolution of sexual system and life-history traits in mosses. *Evolution* 63: 1129–1142.
- Crosby M, Magil RE, He S. 2000. A check list of mosses [online]. Available from <http://www.mobot.org/MOBOT/tropicos/oAmost/checklist.shtml%0A>. [accessed 18 November 2021].
- Crum HA. 2001. *Structural diversity of bryophytes*. Ann Arbor, MI: University of Michigan Press.
- Cunningham CW, Omland KE, Oakley TH. 1998. Reconstructing ancestral character states: A critical reappraisal. *Trends in Ecology & Evolution* 13: 361–366.
- Daniels AED. 1998. Ecological adaptations of some bryophytes of the Western Ghats. *Journal of Ecobiology* 10: 261–270.
- Darriba D, Taboada GL, Doallo R, Posada D. 2012. jModelTest 2: More models, new heuristics and parallel computing. *Nature Methods* 9: 772.
- Dos Santos WL, Maciel-Silva AS, Pôrto KC. 2020. How do sexual expression, reproductive phenology and reproductive success relate to sexual systems in *Fissidens* Hedw. (Fissidentaceae)? A case study comparing two different sexual systems in mosses. *Plant Biology* 22: 573–581.
- During H. 2007. Relations between clonal growth, reproduction and breeding system in the bryophytes of Belgium and The Netherlands. *Nova Hedwigia* 131: 133.
- Edwards SR. 1979. Taxonomic implications of cell patterns in haplolepidous moss peristomes. In: Clarke GCS, Duckett JG eds. *Bryophyte systematics. Systematics Association Special Volume 14*. London: Academic Press. 317: 658–695.
- Endress PK, Baas P, Gregory M. 2000. Systematic plant morphology and anatomy-50 years of progress. *Taxon* 49: 401–434.



- Fedosov VE, Fedorova AV, Fedosov AE, Ignatov MS. 2016. Phylogenetic inference and peristome evolution in haplolepidous mosses, focusing on Pseudoditrichaceae and Ditrichaceae s. l. *Botanical Journal of the Linnean Society* 181: 139–155.
- Felsenstein J. 2004. *Inferring phylogenies*. Sunderland: Sinauer Associates.
- Flora of North America. 2007. Fissidentaceae. In: Flora of North America Editorial Committee ed. *Flora of North America*. Bryophyta, Part 1. Oxford: Oxford University Press. 27: 331–357.
- Folk R, Kates H, LaFrance R, Soltis D, Soltis P, Guralnick R. 2021. High-throughput methods for efficiently building massive phylogenies from natural history collections. *Applications in Plant Sciences* 9: e11410.
- Frey W, Stech M, Meissner K. 1999. Chloroplast DNA-relationship in palaeoaustal *Lopidium concinnum* (Hypopterygiaceae, Musci). An example of steno-evolution in mosses studies in austral temperate rain forest bryophytes 2. *Plant Systematics and Evolution* 218: 67–75.
- Fritsch R. 1991. *Index to bryophyte chromosome counts*. *Bryophytorum bibliotheca*. Berlin-Stuttgart: Cramer. 40.
- Gaff DF, Oliver M. 2013. The evolution of desiccation tolerance in angiosperm plants: A rare yet common phenomenon. *Functional Plant Biology* 40: 315–328.
- Gallenmüller F, Langer M, Poppinga S, Kassemeyer H-H, Speck T. 2018. Spore liberation in mosses revisited. *AoB Plants* 10: plx075.
- Glime J, Vitt D. 1984. The physiological adaptations of aquatic Musci. *Lindbergia* 10: 95–110.
- Glime JM. 2017. *Bryophyte ecology* (Vol. 1). Michigan Technological University and the International Association of Bryologists. Available from <https://digitalcommons.mtu.edu/bryophyte-ecology/> [accessed 18 November 2021].
- Goebel K. 1905. Organography of plants especially of the archegoniate and spermatophyta, part II. *Special Organography*. Oxford: Clarendon Press.
- Goffinet B, Cox C. 2000. Phylogenetic relationships among basal-most arthroodontous mosses with special emphasis on the evolutionary significance of the Funariineae. *The Bryologist* 103: 212–223.
- Hale H, Gardner EM, Viruel J, Pokorny L, Johnson MG. 2020. Strategies for reducing per-sample costs in target capture sequencing for phylogenomics and population genomics in plants. *Applications in Plant Sciences* 8: e11337.
- Hansen TF. 1997. Stabilizing selection and the comparative analysis of adaptation. *Evolution* 51: 1341–1351.
- Harmon LJ, Weir JT, Brock CD, Glor RE, Challenger W. 2008. GEIGER: Investigating evolutionary radiations. *Bioinformatics* 24: 129–131.
- Harvey PH, Pagel MD. 1991. *The comparative method in evolutionary biology*. Oxford: Oxford University Press.
- Heberling MJ, Isaac BBL. 2017. Herbarium specimens as exaptations: New uses for old collections. *American Journal of Botany* 104: 963–965.
- Hedenäs L. 2001. Environmental factors potentially affecting character states in pleurocarpous mosses. *The Bryologist* 104: 72–91.
- Hedenäs L. 2012. Morphological and anatomical features associated with epiphytism among the pleurocarpous mosses—One basis for further research on adaptations and their evolution. *Journal of Bryology* 34: 79–100.
- Hill MO, Preston CD, Bosanquet SDS, Roy DB. 2007. *BRYOATT: Attributes of British and Irish mosses, liverworts and hornworts*. Cambridgeshire: Centre for Ecology and Hydrology.
- Huelsensbeck JP, Ronquist F. 2001. MRBAYES: Bayesian inference of phylogenetic trees. *Bioinformatics Applications Note* 17: 754–755.
- Huerta-Cepas J, Serra F, Bork P. 2016. ETE 3: Reconstruction, analysis, and visualization of phylogenomic data. *Molecular Biology and Evolution* 33: 1635–1638.
- Huttunen S. 2004. Phylogeny and evolutionary relationships of the moss families Brachytheciaceae and Meteoriaceae. *Publications in Botany from the University of Helsinki* 34: 1–33.
- Huttunen S, Bell N, Bobrova V, Buchbender V, Buck W, Cox C, Goffinet B, Hedenäs L, Ho B, Ignatov M, Krug M, Kuznetsova O, Milyutina I, Newton A, Olsson S, Pokorny L, Shaw J, Stech M, Troitsky A, Vanderpoorten A, Quandt D. 2012. Disentangling knots of rapid evolution: origin and diversification of the moss order Hypnales. *Journal of Bryology* 34: 187–221.
- Huttunen S, Bell N, Hedenäs L. 2018. The evolutionary diversity of mosses—taxonomic heterogeneity and its ecological drivers. *Critical Reviews in Plant Sciences* 37: 128–174.
- Huttunen S, Olsson S, Buchbender V, Enroth J, Hedenäs L, Quandt D. 2012. Phylogeny-based comparative methods question the adaptive nature of sporophytic specializations in mosses. *PLOS ONE* 7: e48268.
- Illing N, Denby KJ, Collett H, Shen A, Farrant JM. 2005. The signature of seeds in resurrection plants: A molecular and physiological comparison of desiccation tolerance in seeds and vegetative tissues. *Integrative and Comparative Biology* 45: 771–787.
- Iwatsuki Z. 1977. Bryological miscellanies. *Journal of the Hattori Botanical* 43: 357–364.
- Iwatsuki Z. 1985. A new approach to the classification of the Fissidentaceae (Musci). In: Hara H ed. *Origin and evolution of diversity in plant communities*. Tokyo: Academia Scientific Book. 132–141.
- Iwatsuki Z, Suzuki T. 1977. *Fissidens* in the Ryukyu Islands, Japan. *Journal of the Hattori Botanical* 43: 379–408.
- Iwatsuki Z, Suzuki T. 1982. A taxonomic revision of the Japanese species of *Fissidens* (Musci). *Journal of the Hattori Botanical* 51: 329–508.
- Jesson LK, Cavanagh AP, Perley DS. 2010. Polyploidy influences sexual system and mating patterns in the moss *Atrichum undulatum* sensu lato. *Annals of Botany* 107: 135–143.
- Johnson MG, Granath G, Tahvanainen T, Pouliot R, Stenøien HK, Rochefort L, Rydin H, Shaw AJ. 2014. Evolution of niche preference in *Sphagnum* peat mosses. *Evolution* 69: 90–103.
- Kungu EM, Bonner L, Longton RE. 2003. Patterns of peristome reduction and ornamentation in African Entodontaceae. *The Journal of the Hattori Botanical Laboratory* 93: 223–246.
- LaFarge C, Mishler B, Wheeler J, Wall D, Johannes K, Schaffer S, Shaw AJ. 2000. Phylogenetic relationships within the haplolepidous mosses. *The Bryologist* 103: 257–276.
- Larkin M, Blackshields G, Brown N, Chenna R, McGettigan P, McWilliam H, Valentin F, Wallace I, Wilm A, Lopez R, Thompson J, Gibson T, Higgins D. 2007. Clustal W and Clustal X version 2.0. *Bioinformatics* 23: 2947–2948.
- LANFEAR R, FRANDSEN P, WRIGHT A, SENFELDT T, CALCOTT B. 2016. PartitionFinder 2: New methods for selecting partitioned models of evolution for molecular and morphological phylogenetic analyses. *Molecular Biology and Evolution* 34: 772–773.
- Liu Y, Johnson MG, Cox CJ, Medina R, Devos N, Vanderpoorten A, Hedenäs L, Bell NE, Shevock JR, Aguero B, Quandt D, Wickett NJ, Shaw AJ, Goffinet B. 2019. Resolution of the ordinal phylogeny of mosses using targeted exons from organellar and nuclear genomes. *Nature Communications* 10: 1–11.

- Losos JB. 2008. Phylogenetic niche conservatism, phylogenetic signal and the relationship between phylogenetic relatedness and ecological similarity among species. *Ecology Letters* 11: 995–1003.
- Lowell J. 1998. Drought-adaptation in the leaf-border of *Atrichum undulatum*. *Journal of Bryology* 20: 227–230.
- Lynch M, Gabriel W. 1987. Environmental tolerance. *The American Naturalist* 129: 283–303.
- McDaniel SF, Atwood J, Burleigh JG. 2013. Recurrent evolution of dioecy in bryophytes. *Evolution* 67: 567–572.
- McDaniel SF, Perroud P-F. 2012. Invited perspective: Bryophytes as models for understanding the evolution of sexual systems. *The Bryologist* 115: 1–11.
- Medina NG, Esté A, Banez BN. 2014. Does spore ultrastructure mirror different dispersal strategies in mosses? A study of seven Iberian *Orthotrichum* species. *PLOS ONE* 9: e112867.
- Medina R, Johnson MG, Liu Y, Wickett NJ, Shaw AJ, Goffinet B. 2019. Phylogenomic delineation of *Physcomitrium* (Bryophyta: Funariaceae) based on targeted sequencing of nuclear exons and their flanking regions rejects the retention of *Physcomitrella*, *Physcomitrium* and *Aphanorrhagma*. *Journal of Systematics and Evolution* 57: 404–417.
- Medina R, Lara F, Goffinet B, Garilleti R, Mazimpaka V. 2013. Unnoticed diversity within the disjunct moss *Orthotrichum tenellum* s.l. validated by morphological and molecular approaches. *Taxon* 62: 1133–1152.
- McQueen CB. 1985. Spatial pattern and gene flow distances in *Sphagnum subtile*. *The Bryologist* 88: 333–336.
- Miller MA, Pfeiffer W, Schwartz T. 2010. Creating the CIPRES science gateway for inference of large phylogenetic trees. *Proceedings of the Gateway Computing Environments Workshop (GCE)*, IEEE. 14: 1–8.
- Mishler BD. 1988. Relationships between ontogeny and phylogeny, with reference to bryophytes. In: Humphries CJ ed. *Ontogeny and systematics*. New York: Columbia University Press. 117–136.
- Muggoch H, Walton J. 1942. On the dehiscence of the antheridium and the part played by surface tension in the dispersal of spermatocytes in Bryophyta. *Proceedings of the Royal Society of London, Series B—Biological Sciences* 130: 448–461.
- Müller C. 1848. *Plantae kegelianae Surinamenses. Musci Frondosi, Linnaea* 21: 181–200.
- Müller C. 1851. *Die untrüglichen naturgemäßen Heilkräfte den Kräuter- u. Pflanzenwelt, u. das einfache Le Roi'sche Heilsystem: Mitgeteilt nach Le Roi von Carl Müller*. Oehme u. Müller.
- Müller C. 1900. *Genera Muscorum Frondosorum*. Leipzig: Eduard Kummer.
- Nicolalde-Morejón F, Vergara-Silva F, González-Astorga J, Vovides AP, de los Monteros AE. 2009. Reciprocal illumination of morphological characters upon a molecular hypothesis supports the proposal of a new species of cycad from Mexico. *Systematics and Biodiversity* 7: 73–79.
- Niklas KJ, Kutschera U. 2009. The evolution of the land plant life cycle. *The New Phytologist* 185: 27–41.
- Norkett AH. 1969. Some problems in a monographic revision of the genus *Fissidens* with special reference to the Indian species. *Bulletin of the Botanical Society of Bengal* 23: 75–82.
- Nyholm E. 1986. *Illustrated Flora of Nordic Mosses, Fasc. 1: Fissidentaceae–Seligeriaceae*. Copenhagen & Lund: The Nordic Bryological Society.
- Oliver MJ, Velten J, Mishler BD. 2005. Desiccation tolerance in bryophytes: A reflection of the primitive strategy for plant survival in dehydrating habitats? *Integrative and Comparative Biology* 45: 788–799.
- Olsson S, Buchbender V, Enroth J, Huttunen S, Hedenäs L, Quandt D. 2009. Evolution of the Neckeraceae (Bryophyta): Resolving the backbone phylogeny. *Systematics and Biodiversity* 7: 419–432.
- Orme D, Freckleton R, Thomas G, Petzoldt T, Fritze S, Isaac N, Pearce W. 2013. The caper package: Comparative analysis of phylogenetics and evolution in R. *R Package Version* 5: 1–36.
- Paradis E, Schliep K. 2019. ape 5.0: An environment for modern phylogenetics and evolutionary analyses in R. *Bioinformatics* 35: 526–528.
- Patel N, Medina R, Johnson M, Goffinet B. 2021. Karyotypic diversity and cryptic speciation: Have we vastly underestimated moss species diversity? *Bryophyte Diversity and Evolution* 43: 150–163.
- Pelster PB, van den Hof K, Gravendeel B, van der Meijden R. 2004. The systematic value of morphological characters in *Senecio* sect. *Jacobaea* (Asteraceae) as compared to DNA sequences. *Systematic Botany* 29: 790–805.
- Pokorny L, Ho BC, Frahm JP, Quandt D, Shaw AJ. 2012. Phylogenetic analyses of morphological evolution in the gametophyte and sporophyte generations of the moss order Hookeriales (Bryopsida). *Molecular Phylogenetics and Evolution* 63: 351–364.
- Potier de la Varde. 1931. Études préliminaires de quelques espèces africaines du genre *Fissidens*. *Annales de Cryptogamie Exotique* 2: 272–290.
- Proctor M, Oliver M, Wood A, Alpert P, Stark L, Cleavitt N, Mishler B. 2007. Desiccation-tolerance in bryophytes: A review. *The Bryologist* 110: 595–621.
- Proctor MCF. 1979. Surface wax on the leaves of some mosses. *Journal of Bryology* 10: 531–538.
- Pursell RA. 1966. Two new species of *Fissidens* from eastern Mexico. *The Bryologist* 69: 493–497.
- Pursell RA. 1987. A taxonomic revision of *Fissidens* subgenus *Octodiceras* (Fissidentaceae). *Memoirs of the New York Botanical Garden* 45: 639–660.
- Pursell RA. 1989. Notes on neotropical *Fissidens* I, II, and III. I. The relationship of *F. leptophyllus*. II. The relationship of *F. obtusissimus*, stat. nov. III. The identity of *F. hornsuschii*. *The Bryologist* 92: 523–528.
- Pursell RA. 1994. Taxonomic notes on neotropical *Fissidens*. *The Bryologist* 97: 253–271.
- Pursell RA. 2007. *Fissidentaceae. Flora neotropica monograph*. New York: The New York Botanical Garden.
- Pursell RA, Bruggeman-Nannenga MA. 2004. A revision of the infrageneric taxa of *Fissidens*. *The Bryologist* 107: 1–20.
- Pursell RA, Bruggeman-Nannenga MA, Allen BH. 1988. A taxonomic revision of *Fissidens* subgenus *Sarawakia* (Bryopsida: Fissidentaceae). *The Bryologist* 91: 202–213.
- Pursell RA, Reese WD. 1985. *Fissidens austro-americanus* (Bryopsida: Fissidentaceae), a new species from Brazil and Suriname. *Brittonia* 37: 355–357.
- Qi P, Gimode D, Saha D, Schröder S, Chakraborty D, Wang X, Dida MM, Malmberg RL, Devos KM. 2018. UGBS-Flex, a novel bioinformatics pipeline for imputation-free SNP discovery in polyploids without a reference genome: Finger millet as a case study. *BMC Plant Biology* 18: 1–19.
- R Core Team. 2020. *RStudio: Integrated development for R*. RStudio. Available from <http://www.rstudio.com/> [accessed 18 November 2021].
- Rohrer JR. 1988. Incongruence between gametophytic and sporophytic classifications in mosses. *Taxon* 37: 838–845.

- Rose JP, Kriebel R, Sytsma KJ. 2016. Shape analysis of moss (Bryophyta) sporophytes: Insights into land plant evolution. *American Journal of Botany* 103: 652–662.
- Sayyari E, Mirarab S. 2016. Anchoring quartet-based phylogenetic distances and applications to species tree reconstruction. *BMC Genomics* 17: 101–113.
- Schofield WB. 1981. Ecological significance of morphological characters in the moss gametophyte. *The Bryologist* 84: 149–165.
- Seppelt RD, Stone IG. 2016. *Australian mosses online* 70. *Fissidentaceae*, Version 16. Canberra: Australian Biological Resources Study. Available from [http://www.anbg.gov.au/abrs/Mosses\\_online/70\\_V2\\_Fissidentaceae.html](http://www.anbg.gov.au/abrs/Mosses_online/70_V2_Fissidentaceae.html) [accessed 18 November 2021].
- Seo TK. 2008. Calculating bootstrap probabilities of phylogeny using multilocus sequence data. *Molecular Biology & Evolution* 25: 960–971.
- Sexton JP, Montiel J, Shay JE, Stephens MR, Slatyer RA. 2017. Evolution of ecological niche breadth. *Annual Review of Ecology, Evolution & Systematics* 48: 183–206.
- Shaw AJ, Beer SC. 1997. Gametophyte–sporophyte variation and covariation in mosses. *Advances in Bryology* 6: 35–63.
- Sharp AJ, Crum HA. 1994. The moss flora of Mexico. Pt. 2. *Orthotrichales to polytrichales*. New York: Memoirs of the New York Botanical Garden.
- Shortlidge EE, Rosenstiel TN, Eppley SM. 2012. Tolerance to environmental desiccation in moss sperm. *The New Phytologist* 194: 741–750.
- Smith AJE. 1978. Cytogenetics, biosystematics and evolution in the bryophyta. *Advances in Botanical Research* 6: 195–276.
- Smith AJE, Smith R. 2004. *The Moss Flora of Britain and Ireland*. Cambridge: Cambridge University Press.
- Smith SA, Moore MJ, Brown JW, Yang Y. 2015. Analysis of phylogenomic datasets reveals conflict, concordance, and gene duplications with examples from animals and plants. *BMC Evolutionary Biology* 15: 1–15.
- Stamatakis A. 2014. RAxML version 8: A tool for phylogenetic analysis and post-analysis of large phylogenies. *Bioinformatics* 30: 1312–1313.
- Stanton DE, Reeb C. 2016. Morphogeometric approaches to non-vascular plants. *Frontiers in Plant Science* 7: 916.
- Stark LR. 2017. Ecology of desiccation tolerance in bryophytes: A conceptual framework and methodology. *The Bryologist* 120: 130–165.
- Stech M, Frahm J-P. 1999. The status of *Platyhypnidium mutatum* Ochyra & Vanderpoorten and the systematic value of the Donrichardiaceae based on molecular data. *Journal of Bryology* 21: 191–195.
- Stech M, McDaniel SF, Hernández-Maqueda R, Ros RM, Werner O, Muñoz J, Quandt D. 2012. Phylogeny of haplolepidous mosses—Challenges and perspectives. *Journal of Bryology* 34: 173–186.
- Stone IG. 1987. *Fissidens sufflatus* and *Fissidens pseudopallidus* spp. nov. (Fissidentaceae) from Queensland, Australia. *Memoirs of the New York Botanical Garden* 45: 627–634.
- Stone IG. 1990. *Fissidens*, sections *Crispidium*, *Amblyothallia* and *Serridium* and subgenus *Pachyfissidens* in Australasia: Some taxonomic changes and a key to species. *Journal of Bryology* 16: 245–260.
- Sukumaran J, Holder M. 2010. DendroPy: A Python library for phylogenetic computing. *Bioinformatics* 26: 1569–1571.
- Suzuki T, Inoue Y, Tsubota H. 2018. Molecular phylogeny of the genus *Fissidens* (Fissidentaceae, Bryophyta) and a refinement of the infrageneric classification. *Molecular Phylogenetics and Evolution* 127: 190–202.
- Suzuki T, Iwatsuki Z. 2007. A new approach to the infrageneric classification of the genus *Fissidens* (Fissidentaceae, Bryopsida). *Hikobia* 15: 67–85.
- Thomas A, Igea J, Meudt H, Albach D, Lee W, Tanentzap A. 2021. Using target sequence capture to improve the phylogenetic resolution of a rapid radiation in New Zealand Veronicas. *American Journal of Botany* 108: 1289–1306.
- Vanderpoorten A, Hedenäs L, Cox CJ, Shaw AJ. 2002. Phylogeny and morphological evolution of the Amblystegiaceae (Bryopsida). *Molecular Phylogenetics and Evolution* 23: 1–21.
- Villarreal JC, Renner SS. 2013. Correlates of monoicy and dioicy in hornworts, the apparent sister group to vascular plants. *BMC Evolutionary Biology* 13: 1–8.
- Viruel J, Conejero M, Hidalgo O, Pokorny L, Powell RF, Forest F, Kantar MB, Soto Gomez M, Graham SW, Gravendeel B, Wilkin P, Leitch IJ. 2019. A target capture-based method to estimate ploidy from herbarium specimens. *Frontiers in Plant Science* 10: 937.
- Vitt DH. 1981. Adaptive modes of the moss sporophyte. *The Bryologist* 84: 166–186.
- Wahrmund U, Groth-Maloney M, Knoop V. 2008. Tracing plant mitochondrial DNA evolution: Rearrangements of the ancient mitochondrial gene cluster *trnA-trnT-nad7* in liverwort phylogeny. *Journal of Molecular Evolution* 66: 621–629.
- Wickett NJ, Mirarab S, Nguyen N, Warnow T, Carpenter E, Matasci N, Ayyampalayam S, Barker MS, Burleigh JG, Gitzendanner MA, Ruhfel BR, Wafula E, Der JP, Graham SW, Mathews S, Melkonian M, Soltis DE, Soltis PS, Miles NW, Leebens-Mack J. 2014. Phylotranscriptomic analysis of the origin and early diversification of land plants. *Proceedings of the National Academy of Sciences of the United States of America* 111: e4859–e4868.
- Wilson WG, Harder LD. 2003. Reproductive uncertainty and the relative competitiveness of simultaneous hermaphroditism versus dioecy. *American Naturalist* 162: 220–241.
- Xu B, Ohtani M, Yamaguchi M, Toyooka K, Wakazaki M, Sato M, Kubo M, Nakano Y, Sano R, Hiwatashi Y, Murata T. 2014. Contribution of NAC transcription factors to plant adaptation to land. *Science* 343: 1505–1508.
- Yu G. 2020. Using ggtree to visualize data on tree-like structures. *Current Protocols in Bioinformatics* 69: e96.
- Zastrow E. 1934. Aquatic moss experiments. *Pflanzenforschung* 17: 1–17.

## Supplementary Material

The following supplementary material is available online for this article at <http://onlinelibrary.wiley.com/doi/10.1111/jse.12926/supinfo>:

**Fig. S1.** Fissidentaceae maximum likelihood phylogram based on the analysis of 404 concatenated exon regions (probe data set). This included a total aligned supermatrix of 74 441 nucleotides and 94 partitions, using RAxML with the GTRGAMMA substitution model. Branch lengths are proportional to substitutions per site and support from 1000 rapid bootstrap replicates is indicated by the numbers on the branches.

**Fig. S2.** Fissidentaceae maximum likelihood phylogram based on the analysis of 404 concatenated exons and the flanking regions (full data set). This included a total aligned supermatrix of 493 051 nucleotides and 154 partitions, using

RAxML with the GTRGAMMA substitution model. Branch lengths are proportional to substitutions per site and support from 1000 rapid bootstrap replicates is indicated by the numbers on the branches.

**Fig. S3.** Fissidentaceae species phylogeny. Inferred from 404 RAxML gene trees built from exon regions only (probe data set) using the summary coalescent method ASTRAL-III with each locus treated as a single partition. Branch lengths are in coalescent units ( $2 \times N$  generations), with support values indicating local posterior probability (LPP).

**Fig. S4.** Fissidentaceae species phylogeny. Inferred from 404 RAxML gene trees built from the exon and flanking regions (full data set) using the summary coalescent method ASTRAL-III with each locus treated as a single partition. Branch lengths are in coalescent units ( $2 \times N$  generations), with support values indicating local posterior probability (LPP).

**Fig. S5.** Fissidentaceae species phylogeny. Inferred from 404 RAxML gene trees built from exon regions only (probe data set) using the summary coalescent method ASTRAL-III with each locus treated as a single partition. Branch lengths are in coalescent units ( $2 \times N$  generations), with support values indicating multilocus bootstrap (MLBS) values from 100 replicates.

**Fig. S6.** Fissidentaceae species phylogeny. Inferred from 404 RAxML gene trees built from the exon and flanking regions (full data set) using the summary coalescent method ASTRAL-III with each locus treated as a single partition. Branch lengths are in coalescent units ( $2 \times N$  generations), with support values indicating multilocus bootstrap (MLBS) values from 100 replicates.

**Fig. S7.** Axillary hyaline nodule character states mapped onto the three-gene Fissidentaceae Bayesian inference majority rule consensus tree using maximum likelihood and an equal rates model. The probability of the states at each node is shown as pie charts representing the proportional likelihood values for each character state. The scale bar represents the number of substitutions per site. The legend indicates the color associated with each character state. Species with missing data are in black text. The major clades, which correspond to the numbered branches in Fig. 2, are indicated on the tree.

**Fig. S8.** Limbidium character states mapped onto the three-gene Fissidentaceae Bayesian inference majority rule consensus tree using maximum likelihood and an equal rates model. The probability of the states at each node is shown as pie charts representing the proportional likelihood values for each character state. The scale bar represents the number of substitutions per site. The legend indicates the color associated with each character state. Species with missing data are in black text. The major clades, which correspond to

the numbered branches in Fig. 2, are indicated on the tree.

**Fig. S9.** Peristome morphology character states as defined by Bruggeman-Nannenga & Berendsen (1990) mapped onto the three-gene Fissidentaceae Bayesian inference majority rule consensus tree using maximum likelihood and an equal rates model. The probability of the states at each node is shown as pie charts representing the proportional likelihood values for each character state. The scale bar represents the number of substitutions per site. The legend indicates the color associated with each character state. Species with missing data are in black text. The major clades, which correspond to the numbered branches in Fig. 2, are indicated on the tree.

**Fig. S10.** Continuous character state mapping of the habitat moisture minimum, ranging from 1 (red) to 12 (blue), onto the three-gene Fissidentaceae Bayesian inference tree. The length of the colored scale bar represents the number of substitutions per site. The major clades, which correspond to the numbered branches in Fig. 2, are indicated on the tree.

**Fig. S11.** Continuous character state mapping of the habitat moisture maximum, ranging from 1 (red) to 12 (blue), onto the three-gene Fissidentaceae Bayesian inference tree. The length of the colored scale bar represents the number of substitutions per site. The major clades, which correspond to the numbered branches in Fig. 2, are indicated on the tree.

**Fig. S12.** Continuous character state mapping of the habitat moisture niche breadth, ranging from 1 (red) to 12 (blue), onto the three-gene Fissidentaceae Bayesian inference tree. The length of the colored scale bar represents the number of substitutions per site. The major clades, which correspond to the numbered branches in Fig. 2, are indicated on the tree.

**Table S1.** Herbarium specimens were sampled for phylogenetic analyses.

**Table S2.** Classification systems for species in the genus *Fissidens*.

**Table S3.** Length, informative characters, and evolutionary model for each locus used in Bayesian inference for a three-locus phylogeny.

**Table S4.** Three models of character evolution (“ARD”—all rates different, “SYM”—symmetric, and “ER”—equal rates) were tested for fit using the Akaike information criterion (AIC) and the “fitDiscrete” function in GEIGER (Harmon et al., 2008). Although there is the best fit model for each character (highest AIC value), there is not a statistically significant difference among the fit of the models ( $P$ -value = 0.05) and thus the simplest model (ER) for each character was used for each reconstruction and test for phylogenetic signal.

**Table S5.** Representative statistics for phylogenetically independent comparisons including each possible pair of morphological and habitat traits using the three-locus Bayesian inference phylogeny. Statistics were generated using the function *crunch* in the R package *caper*.